Building Technologies & Urban Systems Division
Energy Technologies Area
Lawrence Berkeley National Laboratory

Anthropogenic heat from buildings in Los Angeles County: A simulation framework and assessment

Yujie Xu, Pouya Vahmani, Andrew Jones, Tianzhen Hong

Lawrence Berkeley National Laboratory, Berkeley, California, USA

Energy Technologies Area
July 2024

10.1016/j.scs.2024.105468

This work was supported by the Assistant Secretary for Energy Efficiency and Renewable Energy, Building Technologies Office, of the US Department of Energy under Contract No. DE-AC02-05CH11231.

Disclaimer:

Sustainable Cities and Society 107 (2024) 105468

Contents lists available at ScienceDirect

Sustainable Cities and Society

journal homepage: www.elsevier.com/locate/scs

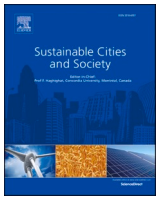

Anthropogenic heat from buildings in Los Angeles County: A simulation framework and assessment

Yujie Xu, Pouya Vahmani, Andrew Jones, Tianzhen Hong *

Lawrence Berkeley National Laboratory, Berkeley, California, USA

ARTICLE INFO

Keywords:
Building anthropogenic heating
Building energy modeling
Urban climate

ABSTRACT

Anthropogenic heat (AH), i.e., waste heat from buildings to the ambient environment, increases urban air temperature and contributes to the urban heat island effect, which leads to more air-conditioning energy use and higher associated waste heat during summer, forming a positive feedback loop. This study used a bottom-up simulation approach to develop a dataset of the annual hourly AH profiles for 1.7 million buildings in Los Angeles (LA) County for the year 2018 aggregated at three spatial resolutions: 450 m, 12 km, and the census tract. Building AH exhibits strong seasonal and diurnal patterns, as well as large spatial variations across the urban areas. Building AH peaks in May and reaches a maximum of 878 W/m^2 within one of several AH hotspots in the region. Among the three major AH components (surface convection, heat rejection from HVAC systems, and zonal air exchange), the surface convection component is the largest, accounting for 78% of the total building AH across LA County. Higher AH is attributed to large building density, a high percentage of industrial buildings, and older building stock. While AH peaks during the day, the resulting ambient temperature increases are much larger during the night. During the July 2018 heatwave in LA County, building AH (excluding the surface component) leads to a daily maximum ambient temperature increase of up to 0.6 °C and a daily minimum ambient temperature increase of up to 2.9 °C. It is recommended that reducing summer building AH should be considered by policy makers in developing mitigation measures for cities to transition to clean energy while improving heat resilience.

1. Introduction

Heat-related mortality and morbidity are on the rise globally and the trend will likely continue with global climate change leading to more intense and longer-lasting heat waves (Perkins-Kirkpatrick & Lewis, 2020; Vahmani, Jones & Patricola, 2019). More than five million people die each year globally because of excessive hot or cold conditions based on a 20-year study (Xu, Ao, Zhao & Pei, 2021). In the 2018 heat wave in Southern California, the UCLA region experienced a record-high temperature of 111 °F (44 °C) on July 6th (Andreatta & Kirksey, 2018) Los Angeles also experienced an all-time high nighttime minimum temperature of 79 °F (26.1 °C) for July (Andreatta & Kirksey, 2018). Such extreme heat events could result in power outages and adverse impacts on public health. It is crucial to investigate strategies to mitigate temperature rises, especially during heatwaves.

AH from the built environment and human activity leads to increased air temperature in the urban environment (Block, Keuler & Schaller, 2004; Vahmani, Luo, Jones & Hong, 2022). This contributes to the urban heat island effect which can lead to heat-related fatalities and morbidity, and strain on the power grid and other urban infrastructure. Human-induced AH comes from four sources (1) buildings, (2) transportation, (3) industrial processes, and (4) human metabolism (Sailor, 2011). The building sector is the major AH contributor, accounting for over half of the total AH (Quah & Roth, 2012; Smith, Lindley & Levermore, 2009). Moreover, building AH is more sensitive to local weather changes, and as a result more susceptible to climate changes. During heat waves, higher outdoor temperatures lead to higher cooling demand which increases energy use and associated heat rejection to the ambient environment from the heating, ventilation, and air-conditioning (HVAC) systems in buildings; the higher heat rejection increases the ambient air temperature, forming a vicious loop (Vahmani et al., 2022). This positive feedback can exacerbate heat-related health damage and also contribute to power outages that can lead to further health and property damage. It is thus crucial to assess building AH and investigate ways to reduce it, especially during heat waves in urban areas.

There are two main approaches to assessing building AH: the top-

* Corresponding author.
E-mail address: thong@lbl.gov (T. Hong).

https://doi.org/10.1016/j.scs.2024.105468
Received 11 January 2024; Received in revised form 21 April 2024; Accepted 22 April 2024
Available online 25 April 2024

Table 1
Comparison of domain size, input resolution, and output resolution among the existing studies.

	Domain Size		Weather Data Resolution			Number of Prototype Building Models					Output Resolution
	Location	Size (square mile)	Source	Grid size	Number of grid points	Residential	Commercial	Institutional	Industrial	other	Duration and resolution
(Chen et al., 2022)	Boston	90	WRF-UCM	1 km		5	11				annual, hourly
(Alhazmi, Sailor & Anand, 2022)	4 major cities	217	TMY	–	4		3				annual, hourly
(Luo et al., 2020)	LA City	502	WRF-UCM	500 m		3	8	1		1	a summer heatwave, hourly
(Hong, Ferrando, Luo & Causone, 2020)	4 major cities	139	TMY3	–	4		16				annual, hourly
(Zheng & Weng, 2018)	LA County	4060	TMY3	–	7		16				annual, hourly
(Nie, Sun & Ni, 2014)	1	1.5	TMY	–	1	1	2	1			annual, hourly
(Zhou, Weng, Gurney, Shuai & Hu, 2012)	Indianapolis City	368	unspecified	–	1	22	8				Noon of June 16, 2001
(Kikegawa et al., 2003)	Otemachi area, Tokyo	0.1	1d UCM	10 km						1	summer, hourly
Current study	LA County	4060	WRF-UCM	12 km	62	9	24	12	9		annual, hourly

down inventory and the bottom-up building energy simulation approach (Sailor, 2011). The top-down approach uses the energy consumption of buildings as a proxy for building heat emissions, assuming building energy and anthropogenic heat are equal in magnitude and there are no temporal lags between them (Sailor, 2011). The energy data are more readily available, making them ideal for large-scale national or international studies. Some re-distribution or downscaling is commonly employed, due to low spatial and temporal resolution of the energy data. The spatial re-distribution usually uses population or GDP data (Dong, Varquez & Kanda, 2017). Sometimes such data are calibrated with other datasets such as night light data representing human activities. Temporal redistribution from monthly data to daily and hourly usually applies some seasonal-specific load profiles (Sailor & Lu, 2004). The top-down approach can produce high-coverage AH datasets; however, many studies have questioned the validity of equating energy and anthropogenic heat. Using energy consumption to represent building AH also neglects the presence of heat emitted from exterior surfaces of buildings through heat convection, which is shown in both the current study and many other studies as the largest building AH component.

Bottom-up approaches calculate anthropogenic heat from individual buildings using detailed building-physics-based models. The results can be aggregated at desired spatial scales. While some studies quantify building AH indirectly using simulated energy consumption as in top-down studies (Zheng & Weng, 2018), or cooling loads (Kikegawa, Genchi, Yoshikado & Kondo, 2003; Wang, Aktas, Malki-Epshtein, Wu & Ammar Bin Abdullah, 2022), the majority of the studies directly simulate AH using building energy models (BEM). These bottom-up approaches require two major inputs, local weather data, and building descriptions that capture its physical systems. configurations and operation patterns. The weather data usually come from either measurement (in actual meteorological year AMY or typical meteorological year TMY) or climate model simulation results using a well-established urban microclimate modeling framework, WRF-UCM. WRF-UCM is an urban microclimate modeling framework coupling the Weather Research and Forecasting (WRF) Model, a state-of-the-art mesoscale climate prediction model, and an urban canopy model (UCM). For simulating building performance, it is usually too data and computation-intensive to create detailed BEMs for each building in a city. Therefore, most bottom-up studies adopt a set of prototype building models to represent all the buildings in the study area. The computation time is a function of the number of weather stations/grid cells, prototype building models, the duration and time-step of simulations, and the amount of simulation output. Due to the high data demand in building stock and local climate, and intense computation requirements, most such studies are only carried out in a smaller geographical domain usually up to a city scale, such as (Chen et al., 2022; Luo, Vahmani, Hong & Jones, 2020). To cover a larger region, tradeoffs need to be made either for the spatial resolution of the weather input, the number of prototype building models, or the simulation run period. Table 1 compares the domain size, input, and output resolutions of eight existing studies and the current study.

Bottom-up studies can analyze the relationship between energy use and AH of buildings, and can further examine building AH components and diurnal profiles. AH from buildings can be grouped into three major components: (1) building envelope surface convection, (2) HVAC operation through heat rejection and relief air, and (3) zone air exchange through exfiltration and exhaust. Hong et al., 2020 conducted a simulation study on the AH and energy consumption for 16 commercial prototype buildings at 4 climate zones and 2 vintages. They found the annual AH to energy consumption ratio differs both by building types, vintages, and climate zones. The ratio ranges from 0.9 to 25.2 and for the majority of buildings, AH is larger than building energy consumption. Alhazmi et al., 2022 evaluated the increased anthropogenic heat caused by the introduction of an office building relative to just the terrain, by excluding terrain AH in the absence of buildings and considering the shade from the building. They found building AH can be as high as 3–4 times the energy consumption for a 6-story office building.

These bottom-up studies have also identified major AH components and compared their relative magnitude. Chen et al., 2022 evaluated the building AH in Boston, MA using a bottom-up approach and prototype building models. They found that the surface component produced the majority of building AH. The ratio between surface, HVAC, and zone AH is 5:4:1 for residential buildings and 7:1:2 for commercial buildings. Hong et al., 2020 examined the ratio by building prototypes and found that while surface convection components accounted for 50% of building AH on average, they range from 13% to 90% across different building types and vintages. Alhazme et al. found for a 2-story office

Table 2
Comparison of the relative contributions of the three AH components and the AH-to-energy ratios, among the existing and this studies.

	Building subsector	AH from Surfaces (%)	AH from HVAC (%)	AH from Zone (%)	AH-to-energy ratio	Time range
(Chen et al., 2022)	Commercial	50	40	10		Annual
	Residential	70	20	10		
(Alhazmi et al., 2022)	Commercial (office)	69	31		2.1–4.44	Annual
(Luo et al., 2020)	Commercial and residential		86.5	13.5		Summer heatwave
(Hong et al., 2020)	Commercial	50 (12.7–90.4)	47.2	2.8 (0.2–11.2)	2.5	Annual
(Zhou et al., 2012)	Commercial and residential				5.8–16.5	1 day in summer
Current study	Commercial	43.3	44.7	12	5.5 (1.3–13.8)	Annual
	Residential	78.7	10.4	10.9	2.1 (0.7–5.6)	
	Industrial	65.5	9	25.5	3.7 (0.6–10.0)	
	Institutional	48.8	46.8	4.4	2.2 (1.1–3.6)	

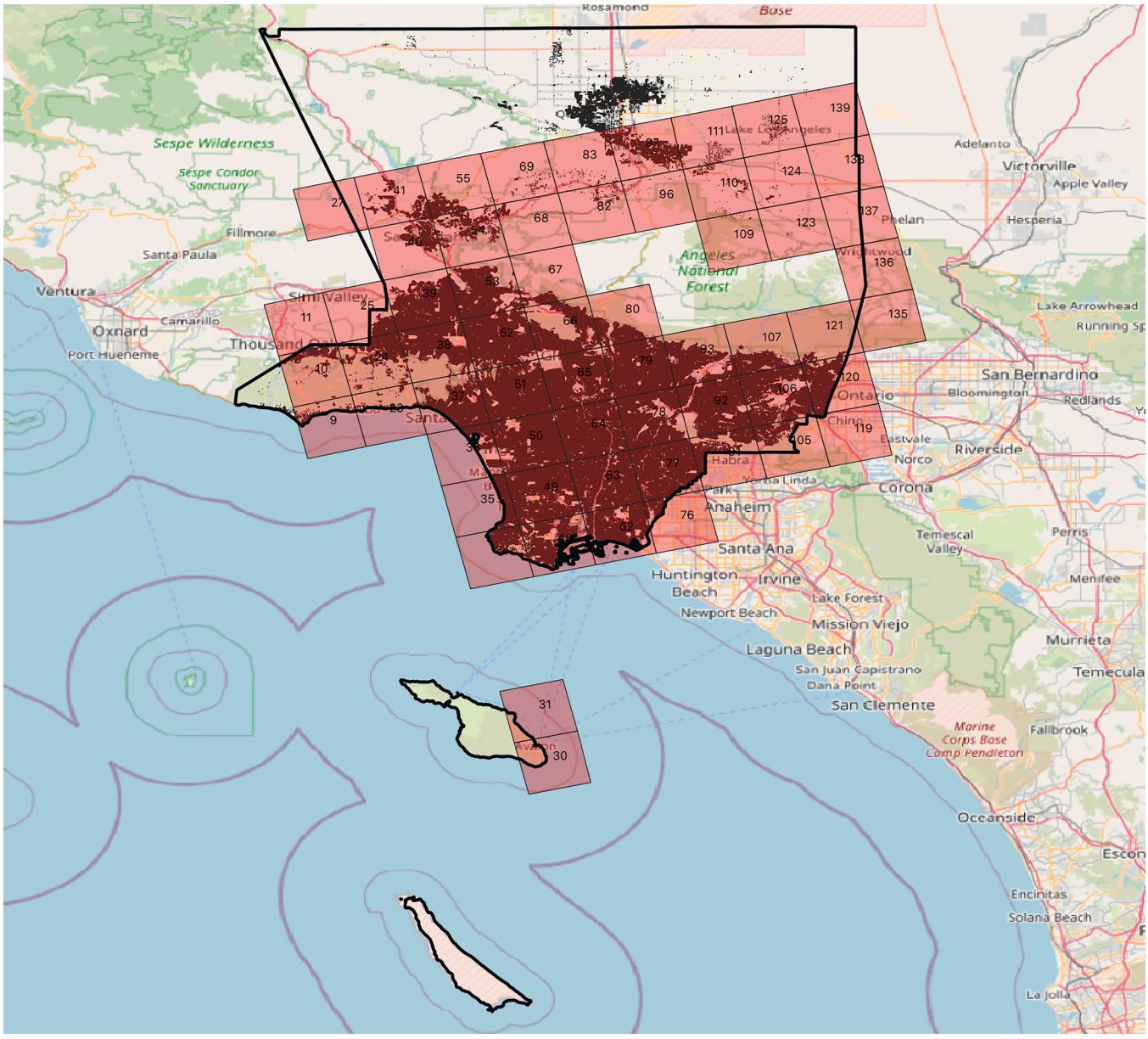

Fig. 1. The 62 WRF grid cells with buildings. The black lines represent the boundary of LA County. The scattered dots represent buildings.

building, the AH from building surfaces is twice that of AH from HVAC operation and argued that since surface convection is the largest contributor of building AH, focusing only on the energy-related AH might not capture the whole picture of building AH and its impact on the ambient environment (Alhazmi et al., 2022). Table 2 compares the compositions of the three major AH components and the building AH-to-energy ratios of five existing studies and the current study.

This paper presents a bottom-up simulation approach and applies it to develop a dataset of AH from buildings in LA County. Detailed analysis was conducted to understand the spatiotemporal characteristics

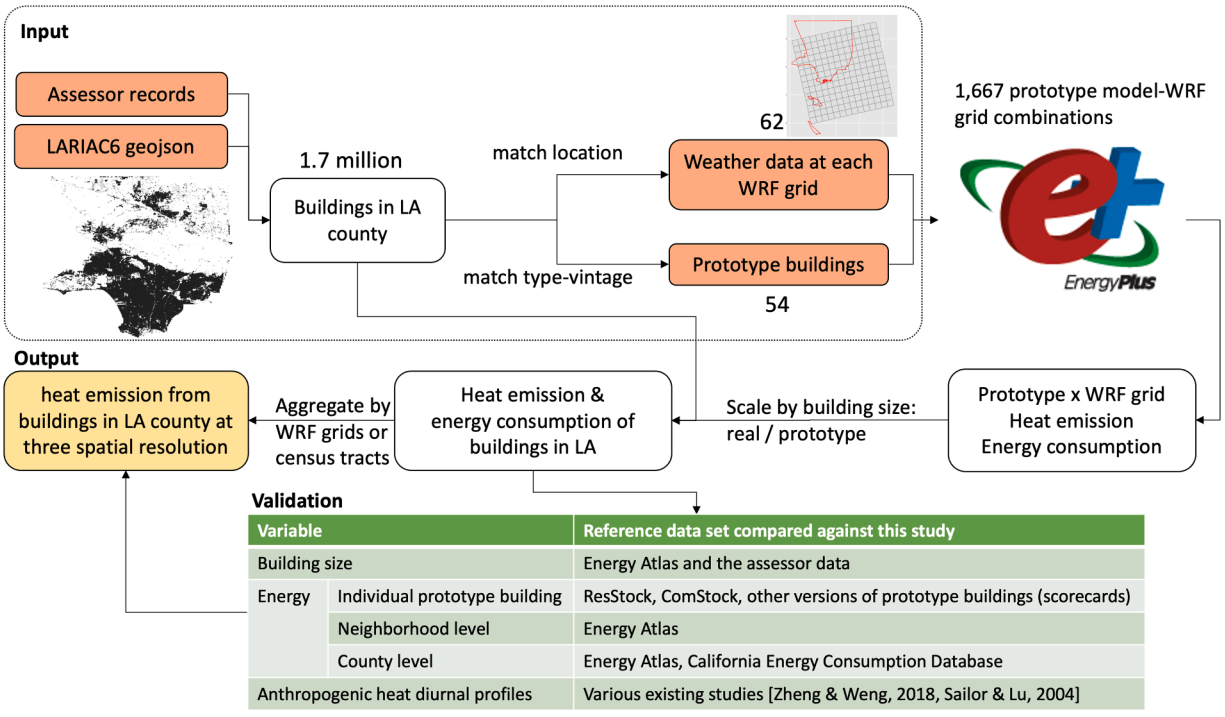

Validation

Variable		Reference data set compared against this study
Building size		Energy Atlas and the assessor data
Energy	Individual prototype building	ResStock, ComStock, other versions of prototype buildings (scorecards)
	Neighborhood level	Energy Atlas
	County level	Energy Atlas, California Energy Consumption Database
Anthropogenic heat diurnal profiles		Various existing studies [Zheng & Weng, 2018, Sailor & Lu, 2004]

Fig. 2. Data and simulation workflow.

of building AH and its impact on the urban environment. The AH dataset was created using physics-based bottom-up building energy models with the EnergyPlus simulation engine (U.S. Department of Energy, 2022). From the simulation results, we examined both the magnitude and timing differences between energy use and anthropogenic heat for different building types. Existing studies mostly focused on the magnitude of the difference except for (Dhakal, Hanaki & Hiramatsu, 2004) but they only analyzed office buildings while the current study covers a wider range of building types.

The current study made the following contributions to the existing body of knowledge:

- The dataset contains a rich high-resolution annual hourly AH from all buildings in LA County in 2018, representing 1.7 million buildings, as compared with the existing bottom-up studies that either cover a smaller domain up to a city, with coarse weather input or consider fewer building types or vintages in the building stock. Furthermore, most existing studies analyze only the commercial building stocks, the current study covers buildings in residential, commercial, institutional, and industrial sectors and also considers different building vintages.
- The dataset aggregates the AH from buildings at three spatial resolutions: the 450 meter (m) x 450 m grid, the 12 kilometer (km) x 12 km grid, and the census tract. With the metadata, it can be aggregated to other spatial resolutions of interest to users.
- Hourly local weather data from WRF-UCM simulations were used as inputs to the building simulation models. The weather inputs are validated with measured weather station data.
- Building AHs from three components were characterized and analyzed in detail across building types and vintages in LA County.
- Seasonal and diurnal patterns of the building AH among 450 m grid cells in LA County were identified; the correlations between building AH and building characteristics such as building type, vintage, and density were evaluated.
- Interactions between building AH and ambient temperature were modeled and evaluated by incorporating AH data (HVAC and Zone components) in high-resolution (450 m) WRF-UCM simulations of urban climate in LA County.

The AH dataset can also be used in similar analysis at other spatial resolutions (census tract, for example), to train statistical or machine learning models for predicting building anthropogenic heat, and to inform urban planning or emergency response strategy through a dashboard visualizing districts or census tracts with the highest AH from buildings that may lead to urban overheating risk and public health issues.

2. Input data and methods

This section describes the data collection, pre-processing, and modeling approaches implemented in the current study.

2.1. The study domain

Los Angeles County has an area of more than 4000 mailes^2 and is one of the most populous areas in the U.S. (U.S. Census Bureau, 2022), hosting a population of about 10 million in 88 cities including the city of Los Angeles. The county has a warm and dry climate (mostly in climate zone 3B). The adjacency to the Pacific Ocean on the southwest side makes the county a transportation hub. It also creates locally different weather with higher humidity and lower temperature variation than the inland area.

2.2. The data and simulation workflow

Fig. 1 shows the study domain with 62 WRF grid cells of 12 × 12 km size which have buildings. LA County has about 1.7 million buildings. It is too compute-intensive to create and simulate detailed BEMs for each of the buildings in the county. Instead, 54 prototype building models (18 building types and 3 vintages, Table 4) were used to represent the LA County building stock based on the building's use type and vintage. Fig. 2 illustrates the data and simulation workflow which uses a bottom-up modeling approach to simulate AH from buildings in LA County and

Table 3
Heat Emission Output Variables from the EnergyPlus Simulation.

Heat Emission Component	EnergyPlus report variable	Variable in the dataset
Zone air exchange	Environment: Site Total Zone Exfiltration Heat Loss [J](hourly)	emission. exfiltration
	Environment: Site Total Zone Exhaust Air Heat Loss [J](hourly)	emission. exhaust
HVAC operation	SimHVAC: Air System Relief Air Total Heat Loss Energy [J](hourly)	emission.ref
	SimHVAC: HVAC System Total Heat Rejection Energy [J](hourly)	emission.rej
Surface convection	Environment: Site Total Surface Heat Emission to Air [J](hourly)	emission.surf

Table 4
Sources of prototype building models used in the current study.

Prototype Building Models	Information Sources
single-family, multi-family	CBES (https://CBES.lbl.gov), generated based on California Title 24 building energy efficiency standards.
heavy and light manufacturing facilities	Adapted from the warehouse models generated by the OpenStudio Standard Gem.
nursing home	Adapted from Sun et al. (2020)
hospital, small hotel, large hotel, small office, medium office, large office, full-service restaurant, stand-alone retail, midrise apartment, primary school, warehouse, college, supermarket	OpenStudio Standard Gem, generated based on ASHRAE 90.1 building energy efficiency standards.
religious worship	Prototype models were developed based on CBECS data (Ye et al., 2019).

produce an hourly building AH dataset. A GeoJSON file was compiled with building geometry and characteristics such as building type, total floor area, number of stories, and vintage (construction year). The climate data were generated from simulations using WRF version 4.2.1 for each of the 62 grids. Next, each building was mapped to a climate grid based on the closest distance between the building footprint polygon's centroid and the grid cell centroid.

The 54 prototype building models were simulated with EnergyPlus for the 62 WRF grid cells, resulting in 1667 valid pairs of prototype-WRF grid cells, using weather files (in EnergyPlus epw format) generated from the WRF simulated climate data. The EnergyPlus simulations produce annual hourly heat emission and energy consumption for each of the prototype-WRF grid pairs, which were used to scale up the results for the entire LA building stock based on the total floor area of buildings by use type and vintage in each WRF grid cell. A validation step was performed by comparing the simulated annual building energy use with other pre-simulated model output for the same climate region, and against a few measured data sources including the CEC Electricity by County database (California Energy Commission, 2020) and the Energy

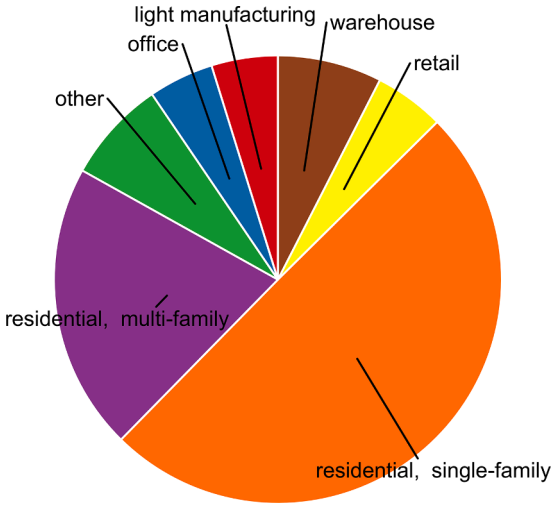

Fig. 4. Building type composition of the compiled LA County building stock data.

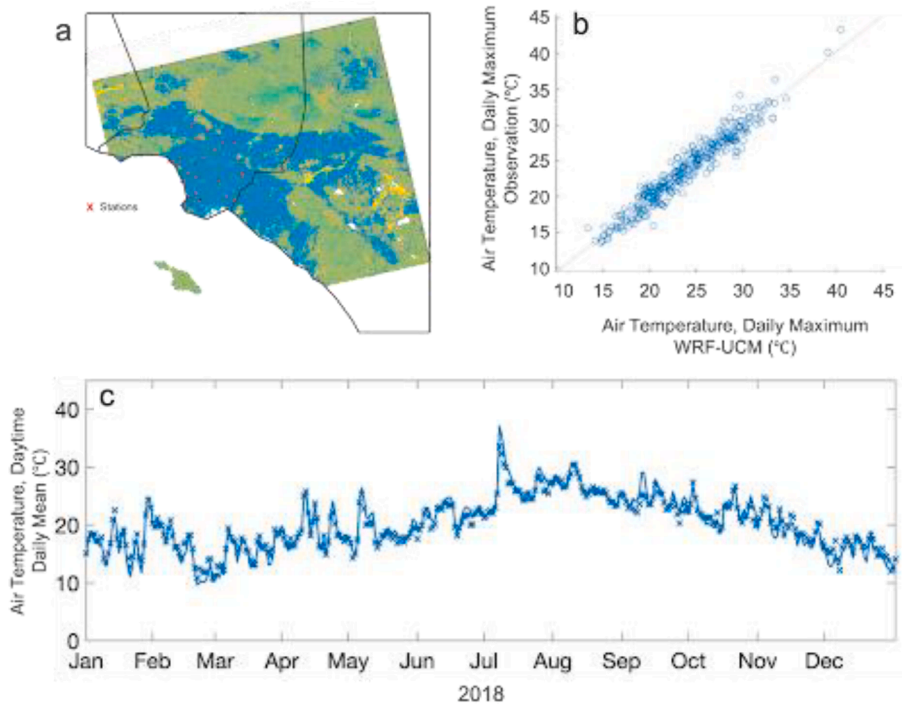

Fig. 3. Location of urban weather stations, within Los Angeles County, used in the validation of WRF-UCM results (a), comparison of ground-based observations and WRF-UCM simulated daily maximum (b), and daytime mean air temperatures (c).

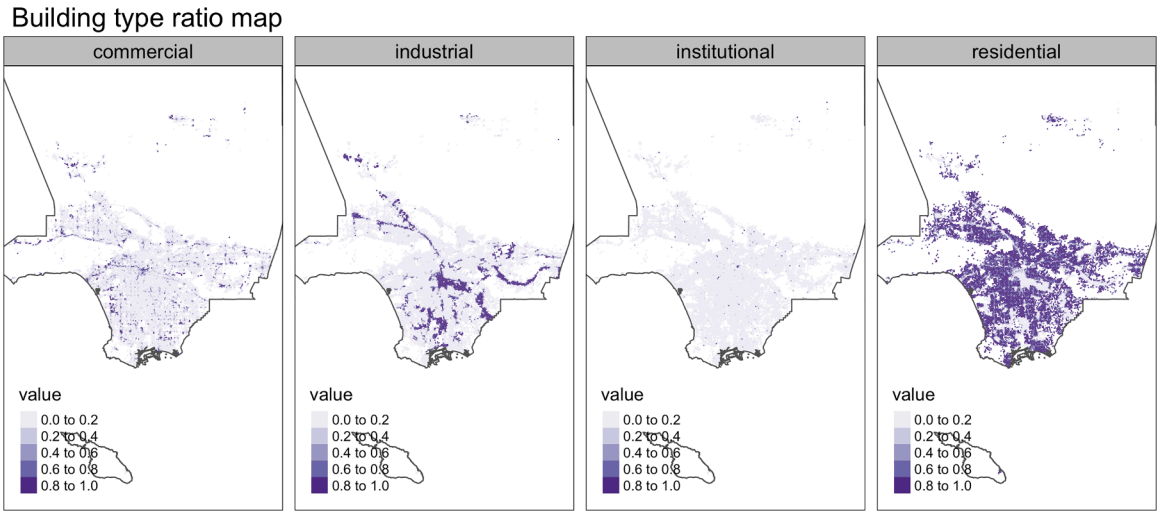

Fig. 5. The ratio of total building floor area in each of the four building subsectors across the 450 m grid cells in LA County.

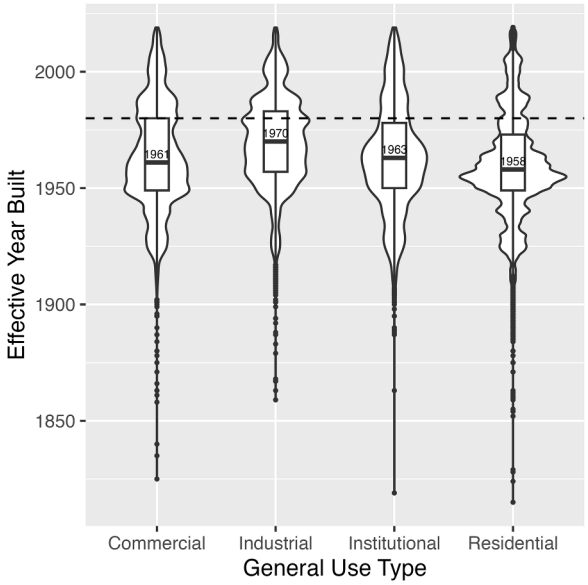

Fig. 6. Year-built distribution of the four building subsectors in the compiled LA building stock data. The dashed line indicates the year 1980.

Atlas (UCLA California Center for Sustainable Communities, 2020). Finally, the AH data was incorporated in a high-resolution (450 m) WRF-UCM modeling framework to analyze the impact of building AH on urban climate. In the end, the AH results were aggregated into three spatial resolutions for buildings in LA County.

2.2.1. *Building energy modeling*

A physics-based approach using the EnergyPlus (U.S. Department of Energy, 2022) simulation engine was adopted to model energy use and heat emissions of buildings. EnergyPlus is the U.S. Department of Energy's flagship building energy software for simulating the dynamic energy and environmental performance of buildings. Building AH is calculated using five output variables (Table 3) representing the different nature of heat emitted from buildings, following the approach of Hong et al., 2020. Each component of heat emissions is calculated with physics-based heat and mass balance equations. The five outputs are aggregated into three major AH components: (1) surface convection - convective heat transfer from the building envelope (exterior walls, roofs, windows) to the urban canopy (hereafter referred to as *envelope convection*); (2) HVAC operation - heat rejection via cooling towers and/or air-cooled condensers, and through relief air from the HVAC systems; (3) Zone air exchange - air mass flow exchange with the ambient air through active exhaust (from kitchen and bathroom fans or window openings) and passive exfiltration (from wall cracks or leaks).

Most of the 54 prototype models in the current study were generated from the OpenStudio Standard Gem (NREL 2022) covering various building types, and vintages for climate zone 3B, to which LA County belongs. Table 4 lists the building prototypes and their information sources. The single- and multi-family building models were generated using the CBES tool (Hong et al., 2015). The nursing home models were adapted from Sun, Specian and Hong (2020) for normal operating conditions. The heavy and light manufacturing facility models were adopted from the warehouse models with their electricity and gas use equipment adjusted to match the statistical ranges of energy use intensity (EUI) from the Manufacturing Energy Consumption Survey (MECS) data (U.S. Energy Information Administration, 2021).

The simulated energy results from the prototype building models were benchmarked against the simulation results from ResStock and ComStock, which is a trusted source of the U.S. building stock performance database.

2.2.2. *WRF climate modeling*

The Weather Research and Forecasting (WRF) model version 4.2.1 (Skamarock et al., 2019) was configured over the Los Angeles metropolitan area to simulate the spatiotemporal variations of urban climate at 12 km resolution for all 365 days in 2018 to provide weather data for the building energy modeling. The WRF model is a state-of-the-science, fully compressible, non-hydrostatic, mesoscale numerical weather prediction model with customizable physical parameterization configurations. We configured WRF with the Rapid Radiative Transfer Model (Iacono et al., 2008) for shortwave and longwave radiation; the Mellor-Yamada-Janjic scheme (MYJ) for Boundary Layer Scheme (Janjić, 1994; Mesinger, 2010); the Thompson scheme (Thompson, Field, Rasmussen & Hall, 2008) for microphysics; and the Eta Similarity scheme (Monin & Obukhov, 1954) for the surface layer. High-resolution National Land Cover Data (NLCD) (Homer, Fry & Barnes, 2012) is used to represent land use and land cover. The ERA5 global reanalysis (Hersbach et al., 2020) data were used as the initial and boundary conditions.

The WRF model was further coupled to a single-layer urban canopy model (UCM) (Kusaka, Kondo, Kikegawa & Kimura, 2001; Yang et al., 2015) to account for urban canopy processes and the interactions between urban surfaces and atmospheric dynamics. The

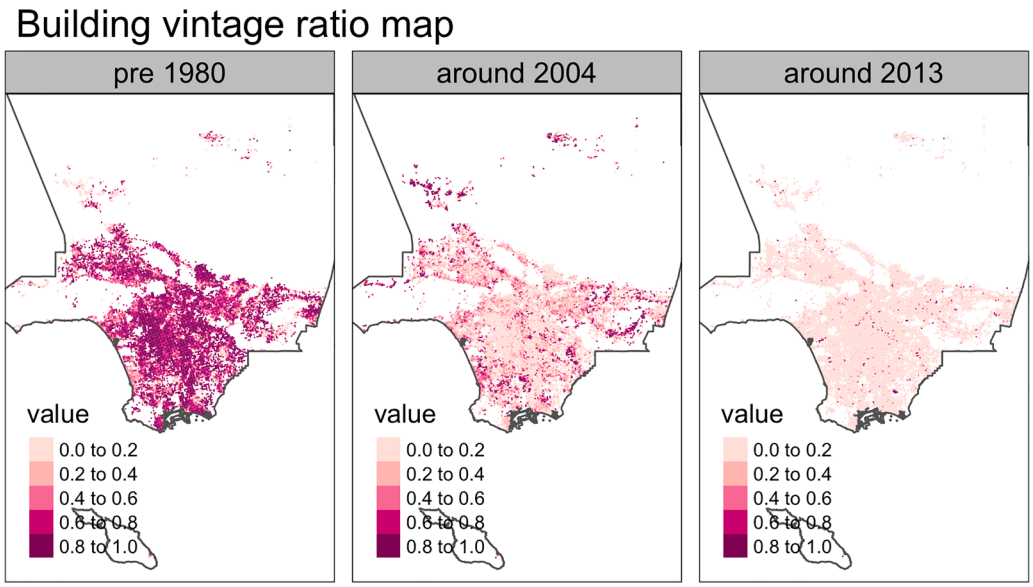

Fig. 7. The ratio of the total building area in each building vintage across the 450 m grid cells in LA County.

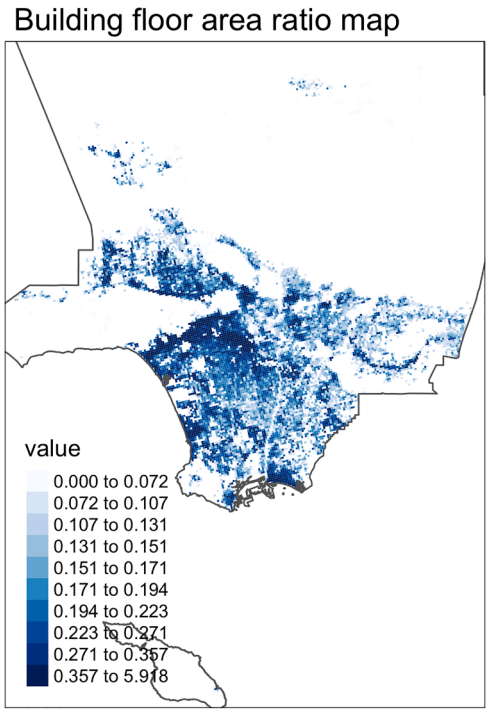

Fig. 8. Building floor area ratio across the 450 m grid cells in LA County.

UCM-parameterized wind profile and radiation processes (e.g., shadowing, reflection, and trapping) inside street canyons, account for the three-dimensional nature of buildings, and resolve wind profiles within street canyons (Chen et al., 2011). The urban morphological parameters (e.g., building height and road width) are defined based on the National Urban Database and Access Portal Tool (NUDAPT) (Ching et al., 2009) dataset. Furthermore, the NLCD impervious surface data (Wickham et al., 2013) were used for an accurate representation of urban fractions. The described WRF-UCM configuration is validated over Los Angeles County against ground-based observations of air temperatures which shows the model reproduces variations of the near-surface air temperature with a root-mean-square error (RMSE) of 1.1 °C (Fig. 3).

WRF-UCM with the same configuration is used a second time to simulate the impacts of AH on outdoor air temperature at 450 m resolution for July only by comparing two scenarios, with and without incorporating spatially distributed hourly AH data.

2.3. Input data summary

2.3.1. Building stock

After the data cleaning and tidying steps, 1.7 million buildings were identified with a footprint and relatively complete data. Fig. 4 shows the contribution of each major building type's total building area (sum of areas of all floors in a building) to the compiled building stock data. There are over 100 distinct building use types listed in the LA County's tax assessor dataset. The types with less than 3% of the building stock are grouped into "other" in the pie chart. Close to half of the building stock is single-family homes, followed by multi-family buildings. Warehouses, light manufacturing facilities, retail stores, and offices each have about 5% of the building stock.

Fig. 5 shows the ratio of building area in each of the four building subsectors. Most climate grid cells are dominated by residential buildings. Industrial buildings are concentrated near Los Angeles downtown, major airports (LBA, LAX, Goodyear Blimp Base Airport), and major roads (CA 60, interstate 5). Commercial and industrial-dominated grids are scattered throughout the county.

The LA County building stock is old. Fig. 6 shows the distribution of the construction year of major building types in the county. For four building subsectors, about 75% of the buildings were built before 1980. Industrial buildings are slightly newer, with a median construction year of 1970, about 10 years newer than the other three types. Based on the data summary and California building energy efficiency standards Title 24's three-year release cycles, the following three vintages were selected to group the building stock: (1) before 1980 (no efficiency requirements), (2) around 2004, and (3) after 2013. From the vintage map in Fig. 7, we can see that the majority of the grid cells, especially the central area of the county, are dominated by old buildings. Newer buildings are mainly near coastal areas or major roads.

The overall building area ratio (the total building floor area divided by the area of the climate grid cell) is shown in Fig. 8. The highest building coverage is around Los Angeles downtown in the center, Hollywood in the central west, Long Beach along the west coast, and Hermosa Beach along the south coast.

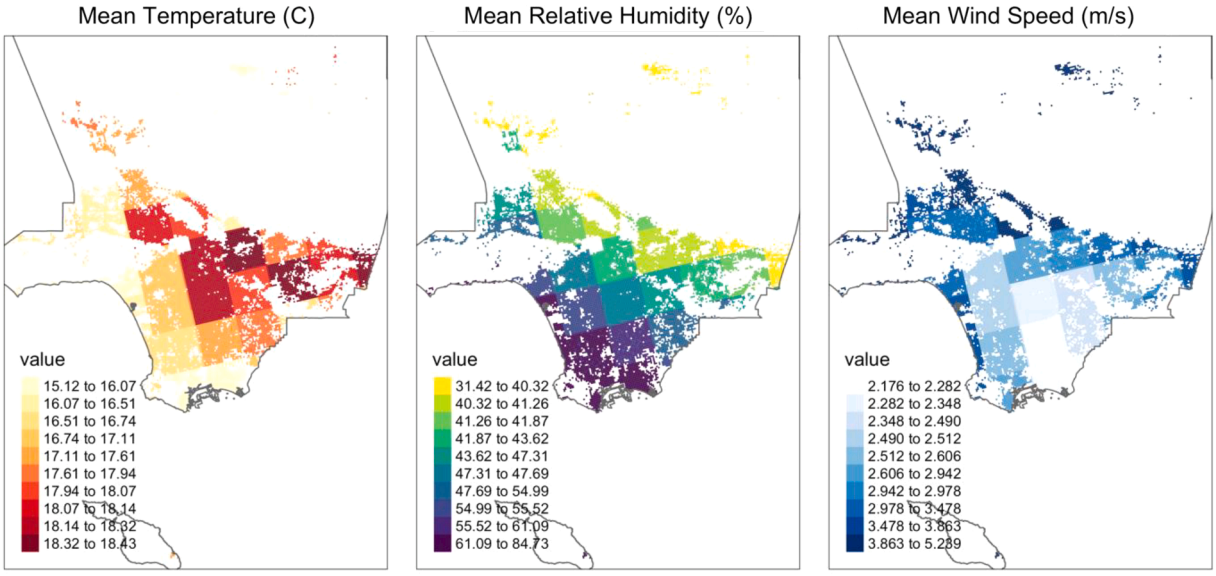

Fig. 9. Maps of the annual average temperature (left), relative humidity (middle), and wind speed (right).

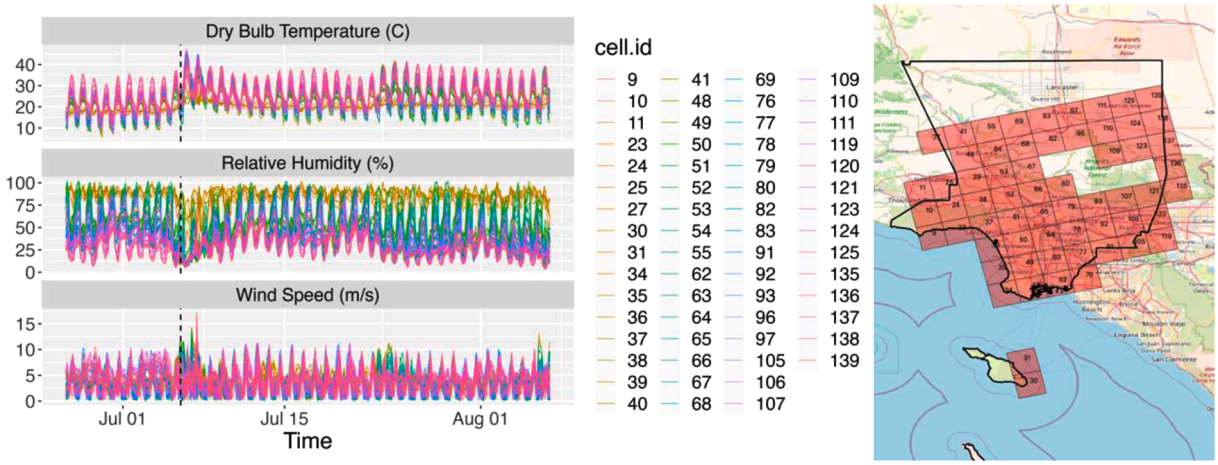

Fig. 10. Outdoor dry bulb temperature, relative humidity, and wind speed of grid cells with valid building data (Left). WRF grid cell IDs and location (Right).

Table 5
Percentages of the three building AH components, among four major building sectors and across the county. "< 1980", "2004", and "2013" corresponding to three building vintages.

Building Use Type	Surface Convection AH (%)			HVAC AH (%)			Zone AH (%)		
	vintage			vintage			vintage		
	< 1980	2004	2013	< 1980	2004	2013	< 1980	2004	2013
residential	73.4	80.7	83.9	14.8	9.8	4.5	11.8	9.5	11.6
commercial	48	39.9	42.2	38.7	49.4	45.8	13.3	10.7	12.1
industrial	70	58.9	68.8	6.2	13.4	6.3	23.8	27.8	24.8
institutional	41.3	40.9	38.2	50.4	55.7	57.9	8.3	3.4	3.9
residential (all vintages)	78.7			10.4			10.9		
commercial (all vintages)	43.3			44.7			12		
industrial (all vintages)	65.5			9			25.5		
institutional (all vintages)	48.8			46.8			4.4		
The average across all prototypes	55.9			31.6			12.5		
Across LA county	78.2			10.8			11.0		

2.3.2. Weather data

The weather data were provided at the 12 km x 12 km grid cells. Fig. 9 shows the annual average temperature, relative humidity, and wind speed in LA County. The weather condition in LA County exhibits clear coastal-inland differences, where the coastal area is cooler, more humid, and windier than the inland area. A windy area is also present near the mountainous region in the northeast of the county.

Fig. 10 shows that the WRF climate data for July 2018, with a

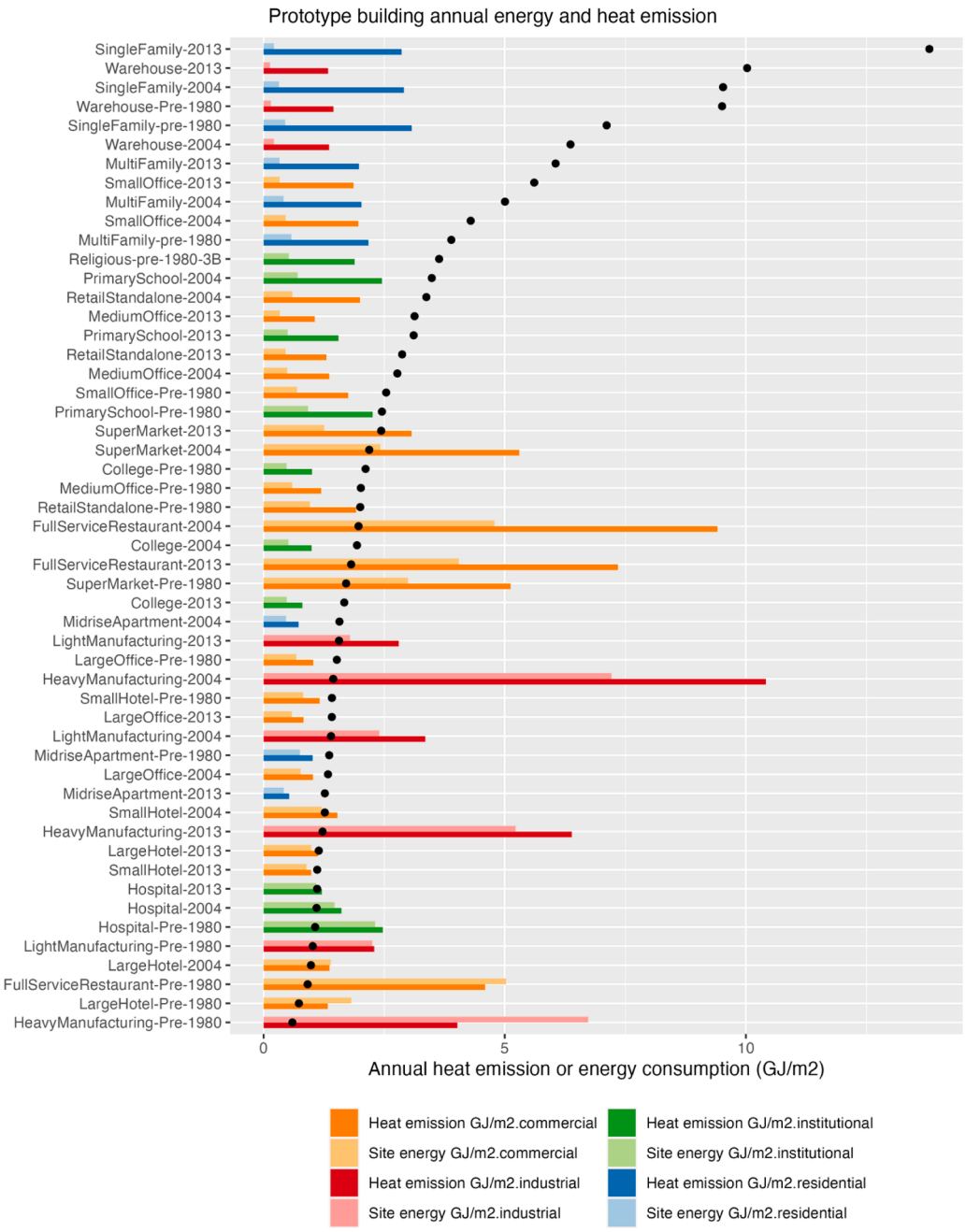

Fig. 11. Annual total anthropogenic heat (lighter colored bars) and energy consumption, both normalized by the total building floor area, of electricity and gas (darker colored bars) among the prototype models, averaged across different weather inputs at different grid cells. The dots are the AH-to-energy ratios for each prototype building.

heatwave starting on July 6, has a visible peak, highlighted by the dashed line. There are also some interesting coastal and inland differences. The yellow lines show the weather trends for coastal grids such as 34, 35, and 36. They exhibit a low variation in temperature and a high variation in relative humidity (RH). On the contrary, the pink lines of inland grids (with IDs above 120) display high variations in temperature and low variations in RH.

3. Results

This section summarizes and analyzes the simulated AH data at the 450 m grid cell resolution over LA County. Data of the other two resolutions can be found in the dataset made available to the public (See Section 6).

3.1. Relationship between building energy use and anthropogenic heating

This section compares the magnitude, temporal profiles, and effect of building vintages (indication of energy efficiency level), which addresses the research question of whether building energy consumption can be directly used to represent building AH, a common practice in many top-down building AH studies (see Section 1).

3.1.1. AH-to-energy ratio

In majority of cases, building AH is larger than its energy consumption, with the AH-to-energy ratios varying widely from 0.6 to 13.8. Residential buildings and warehouses have the highest heat-to-energy ratios, especially for the newest single-family homes, their annual heat emission is about 14 times the annual energy consumption. This is likely

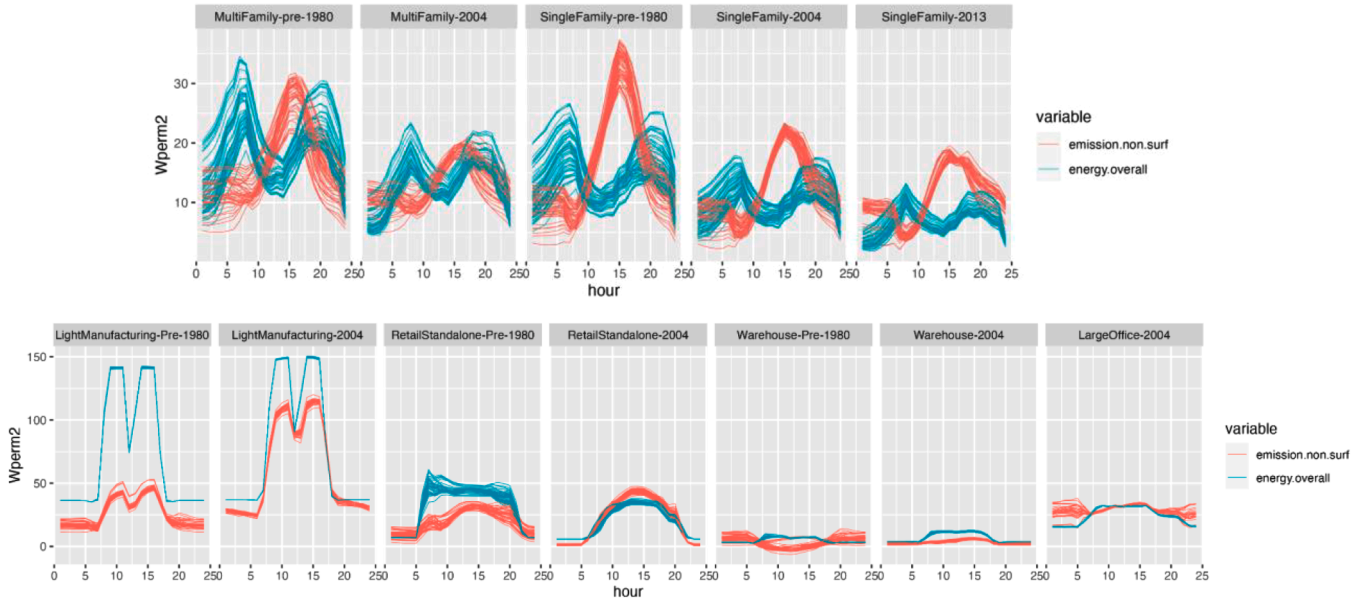

Fig. 12. Diurnal profile of prototype non-surface component building anthropogenic heat vs energy consumption for residential buildings (top row) and non-residential buildings (bottom row). The total building non-surface AH is the sum of the HVAC and zone AHs. Different lines represent results from different weather inputs.

due to the high contribution of surface AH component (see Section 33), which is less related to the occupant's energy-using behavior. When excluding the largest AH component from the building surface convection, the ratios become much smaller, ranging from 0.3 (Heavy Manufacturing pre-1980) to 1.9 (Medium Office 2013). Among the prototype buildings, industrial and commercial buildings have the highest heat emission and energy use intensity among the prototype building models. This analysis extends (Hong et al., 2020) by including residential and industrial prototype buildings and an older pre-1980 vintage.[1] Heavy manufacturing facilities, full-service restaurants, and supermarkets are the buildings with the highest heat emissions. These buildings tend to have high energy consumption as well.

3.1.2. *Diurnal AH profiles*

When the surface component is excluded from the total AH, the remaining annual building AH is more similar to its energy consumption. However, by comparing the diurnal profiles of the non-surface AH with the energy consumption (Fig. 12), we can see that there is a clear shape difference in residential buildings where the energy consumption has two peaks, one around 8am and one around 8pm while building AH has only one peak around 3pm. The diurnal profile shapes are more similar in non-residential buildings such as manufacturing facilities and retail stores. For large offices and warehouses, the HVAC + Zone AHs are flatter than the energy consumption. In terms of the variability due to weather conditions, residential buildings have similar weather variability in energy consumption and HVAC + Zone AH, while for non-residential buildings, AHs tend to have larger weather-induced variabilities than energy use.

3.1.3. *Building vintage*

To compare building anthropogenic heat and energy use among different building vintages, we examined the distribution of the changes in anthropogenic heat or energy use from the pre-1980 vintage to the 2004 (or 2013) vintage (Fig. 13). A negative value suggests a decrease in anthropogenic heat or energy use in the newer buildings. The variability within each boxplot is due to differences in the input weather files. For residential buildings and hospitals, newer buildings show reductions in both anthropogenic heat and energy use compared with older buildings. Specifically, compared with the pre-1980 vintage, single and multi-family buildings have a 5–10% reduction in building AH and a 25–50% reduction in their energy consumption in the 2004 and 2013 vintage. For full-service restaurants and small offices, newer buildings have lower energy consumption but higher anthropogenic heat compared with their pre-1980 counterparts. For supermarkets, retail stores, large offices, large hotels, and manufacturing facilities, newer buildings lowered energy consumption in both 2004 and 2013 vintages but only the 2013 vintage saw anthropogenic heat reduction. The differences in the effect of newer buildings on energy and AH likely stem from the differences in the type of energy efficiency upgrades. For example, the newer full-service restaurants have better lighting and appliances and achieve major reduction in lighting energy and electricity and gas equipment consumption; while the main contributor to the increased AH in newer full-service restaurants is the increased maximum flow rate of the exhaust fan.

3.2. *Components of building anthropogenic heat*

Buildings produce anthropogenic heat in three major channels: surface convection, HVAC operation through rejection and relief air, and zone air exchange through exfiltration and exhaust. Building surface convection is the major contributor to building AH across all building sectors except for commercial buildings where HVAC and surface convection are comparable. In residential buildings, close to 80% of the AH is from surface convection. The surface-HVAC-Zone AH ratios are similar between the residential sector and the whole of LA County as it is the dominant building use type (see Table 5).

3.2.1. *Building vintage*

On average, newer buildings, although consuming less energy due to higher energy efficiency level, have slightly relative higher HVAC contribution in total AH. Although vintage is secondary as compared with building type in determining the AH percentage composition. The contribution of the HVAC component in total AH is increased in newer

[1] GJ/m^2 is used as the unit of measure following Hong et al. 2022 for an easier cross comparison. Note that GJ/m^2 can be converted to kWh/m^2 by multiplying 277.78

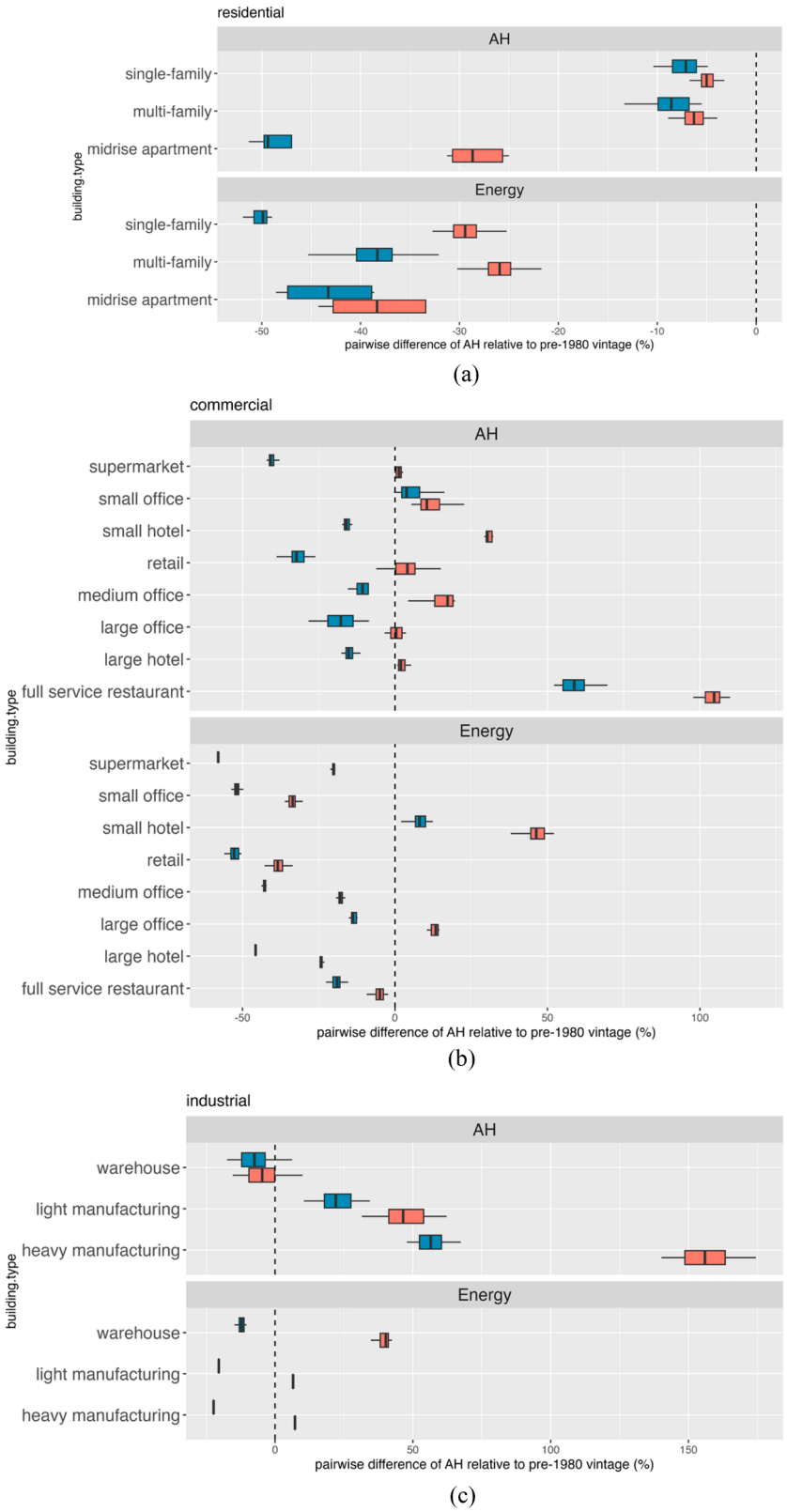

Fig. 13. Distribution of building anthropogenic heat and building energy consumption difference between the 2004 and pre-1980 vintage (red) and difference between the 2013 vintage and pre-1980 vintage (blue), for residential (a), commercial (b), industrial (c), and institutional buildings (d).

vintages for commercial and institutional buildings and decreased for residential buildings. Across different building types, warehouses have the largest percentage of surface AH, while large offices lead in HVAC AH, and full-service restaurants have the highest percentage of AH from zone air exchange.

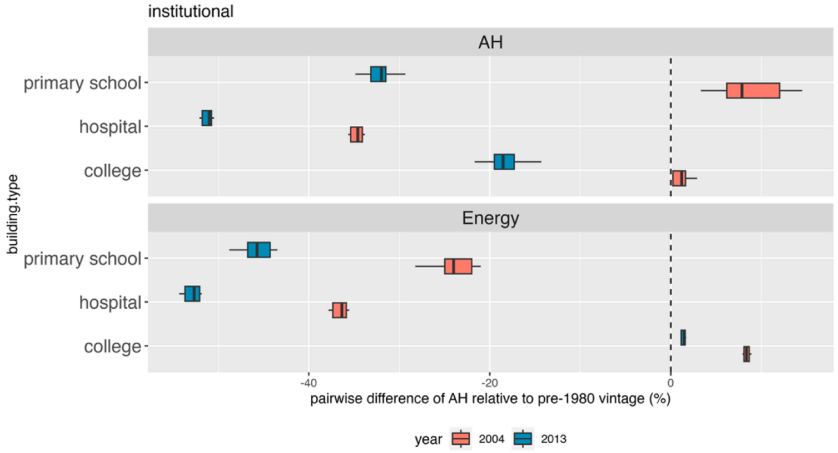

(d)

Fig. 13. (*continued*).

3.2.2. Diurnal profile across seasons

This section breaks down the seasonal diurnal profiles into the three AH components and compares them side-by-side with three relevant weather variables (Fig. 14). The surface component peaks at noon and drops below zero at night, resembling the diurnal profile of solar radiation. The HVAC and Zone AH components are more correlated to temperature and wind speed. Although the outdoor temperature peaks around noon, the indoor is not heated up right away. This time lag is due to the thermal mass, building insulation level, air tightness, etc., and as a result, the peak cooling loads and associated HVAC energy use and AH are about two hours after the outdoor temperature peak. Zone anthropogenic heat follow the overall urban temperature curve but also resembles the wind speed pattern in the dips in the morning. The dip around noon time matches the infiltration schedule of the manufacturing facilities, which are among the highest heat emission building types (See Fig. 11). Zone exhaust and exfiltration-induced AH is highest in colder months like spring and winter, as opposed to HVAC and surface AH which are larger in summer. The zone's anthropogenic heat is larger in spring than in winter, likely due to higher wind speed.

3.2.3. Spatial distribution

This section compares the spatial distribution of four snapshots of building anthropogenic heat in summer at noon and night on a weekday and a weekend day, for the surface component and non-surface components (Fig. 15). The similarity in the spatial layout of hot spots among the four daytime maps suggests that non-time-varying factors like building type and vintage composition, location which are indicative of the climate condition, are more decisive in the rankings of anthropogenic heat than temporal factors. The anthropogenic heat from surface convection has a very clear day-night difference, echoing the diurnal profiles in Fig. 14. The surface-AH component has a larger day-night difference than the non-surface AH. Among the four weekday-weekend pairs, non-surface AH during the weekend night is larger than weekday night, especially around Beverly Hills and along West Hollywood, suggesting heavier human activity during weekend nights.

3.3. Correlation of peak building anthropogenic heat with the building stock characteristics

By comparing the maps of building anthropogenic heat and building stock in Section 2.3.1, we can see a strong correlation between building floor area ratio and anthropogenic heat. The industrial regions also collocate with higher anthropogenic heat regions. A more systematic regression analysis was conducted to examine the correlation between building stock characteristics and building anthropogenic heat, using the specification in Eq. (1).

$$AH_{ij} = \alpha + \left(\gamma_{0j} rcom_i + \gamma_{1j} rres_i + \gamma_{2j} rind_i\right) + \mu_j FAR_i + \left(\lambda_{0j} vin04_i + \lambda_{1j} vin13_i\right) \quad (1)$$

$AH_{i,j}$ is the annual peak anthropogenic heat flux of the jth component (overall, surface convection, HVAC, and zone) for 2018, for the i th 450 m grid cell. $rcom_i$, $rres_i$, and $rind_i$ are the ratios of building floor area that are commercial, residential, or industrial in grid cell i. The ratio of institutional buildings is left out as a reference group to prevent multicollinearity in model fitting. FAR_i is the total building area divided by the total grid area for grid cell i. $vin04_i$ and $vin13_i$ are the ratios of buildings built around 2004 or 2013 in grid cell i. The pre-1980 vintage ratio is left out as a reference group to prevent multicollinearity.

The estimated regression coefficients specified in eq (1) are shown in Table 6. For the overall and surface anthropogenic heat, higher industrial and commercial building ratios, and large building floor area ratios are associated with higher anthropogenic heat. Compared with institutional buildings, a higher residential ratio is associated with lower anthropogenic heat. Specifically, holding other factors constant, when one grid cell has one percent higher industrial buildings and one percent lower institutional buildings, the former tends to have 44.6 W/m^2 higher peak building anthropogenic heat than the latter. When other factors are the same, one grid cell has one percent more residential buildings and one percent fewer institutional buildings than another grid cell, the annual peak building anthropogenic heat is likely to be 14.1 W/m^2 lower than the latter. One percent higher floor area ratio is associated with 208.8 W/m^2 higher building anthropogenic heat. Compared with pre-1980 buildings, newer buildings tend to have lower anthropogenic heat. Specifically, holding other characteristics the same, when one grid cell has one percent higher 2004-vintage buildings and one percent lower pre-1980 buildings, the former is likely to have 11.7 W/m^2 lower annual peak building anthropogenic heat. When the former has one percent higher vintage-2013 buildings and one percent lower pre-1980 buildings than the second grid, the former tends to have 14.7 W/m^2 lower annual peak anthropogenic heat. Note that the coefficients only provide a summary of the data and should not be interpreted as causal.

Unlike the other three components, a higher ratio of industrial buildings is associated with lower HVAC-related anthropogenic heat, probably because the HVAC conditioning needs in industrial buildings are overshadowed by the industrial process needs, lighting, etc. For the Zone air exchange-resulted anthropogenic heat, the association between the anthropogenic heat and the ratio of commercial and residential buildings, and the 2004 vintage ratio are not statistically significant.

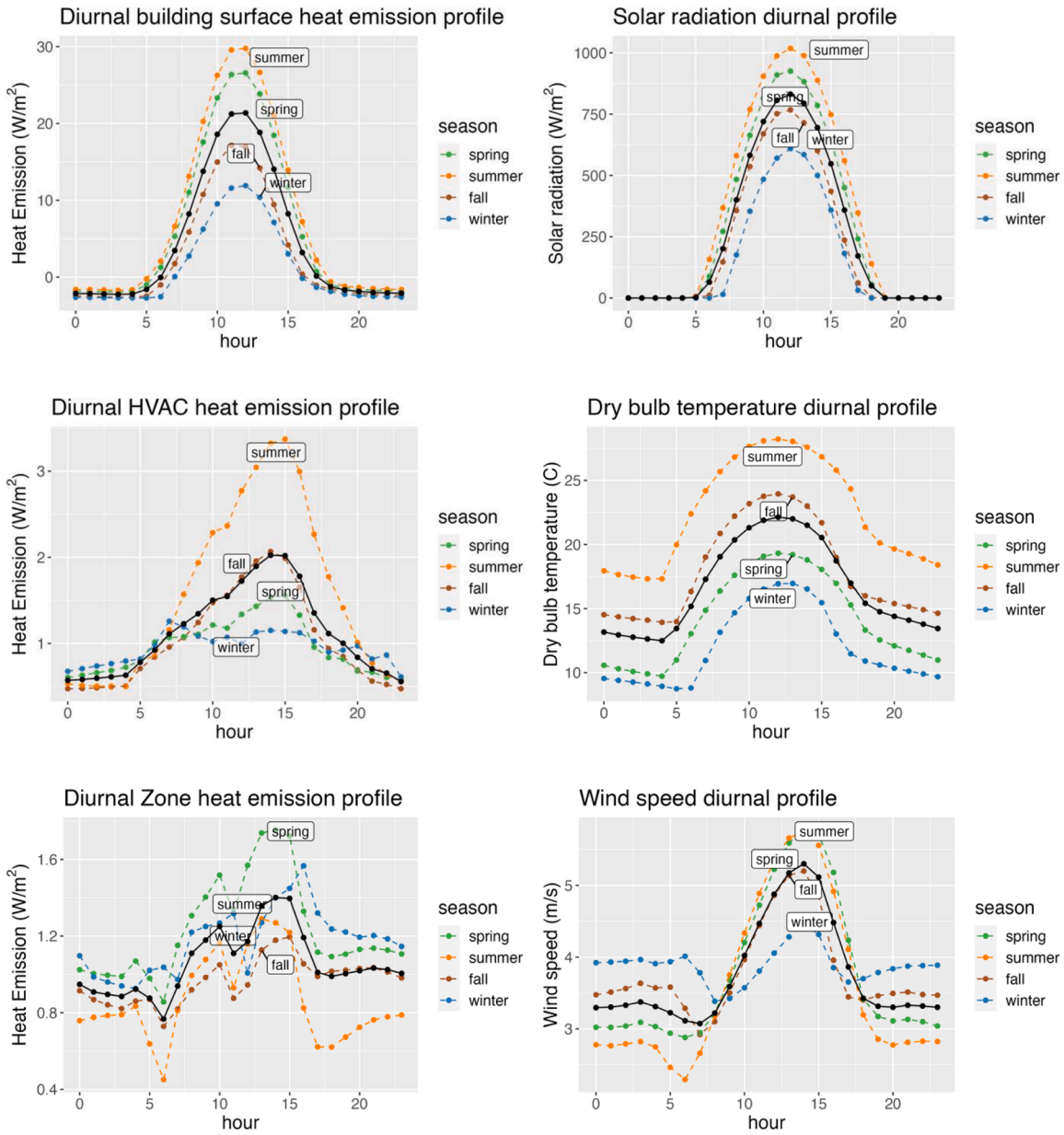

Fig. 14. Diurnal profile of total building anthropogenic heat (top left), three building anthropogenic heat components (middle), relevant environment, and building factors (right column and bottom left). Each color represents a season in 2018. The black line is the average diurnal profile of all seasons.

3.4. Correlation between HVAC and zone building anthropogenic heat and outdoor air temperature

HVAC-resulted building anthropogenic heat is linearly correlated with outdoor air temperature between 20 °C and 30 °C (Fig. 16). When it is 20 °C outside, the HVAC-induced AH is minimal as it's around the comfortable temperature and little cooling or heating is required by buildings; it increases when outdoors is colder or hotter. However, when the daily peak outdoor air temperature is above 32 °C (close to LA's summer design day outdoor air temperature of 32.2 °C/90 °F), the anthropogenic heat starts to plateau, which is likely a result of cooling demand exceeding cooling capacity on sweltering days during heat waves.

In summer, the plateau behavior at high temperatures exhibits heterogeneity among different building types (Fig. 17). Residential buildings all have the plateau behavior while non-residential buildings show more irregularity and flatter AH-temperature curves. The changepoint temperatures for residential buildings are all around 32 °C but pre-1980 residential buildings have higher HVAC-induced AH than newer ones due to the higher cooling loads thus energy use of the energy-inefficient older homes.

Zone air-exchange-resulted anthropogenic heat decreases with outdoor air temperature (Fig. 18). In summer, outdoor air temperature is usually higher than indoor temperature. The indoor-outdoor air exchange makes buildings absorb heat (or emit negative heat). When outdoor temperature increases, the indoor-outdoor temperature difference increases, and the absorbed heat increases, which is equivalent to the emitted negative heat decrease. In winter, indoor air temperature is usually higher than the outdoor air temperature, and buildings release heat through indoor-outdoor air exchange. When the outdoor air temperature increases, indoor-outdoor temperature decreases, causing a reduction in the heat released through air exchange. In both situations, an increase in outdoor air temperature leads to a decrease in anthropogenic heat.

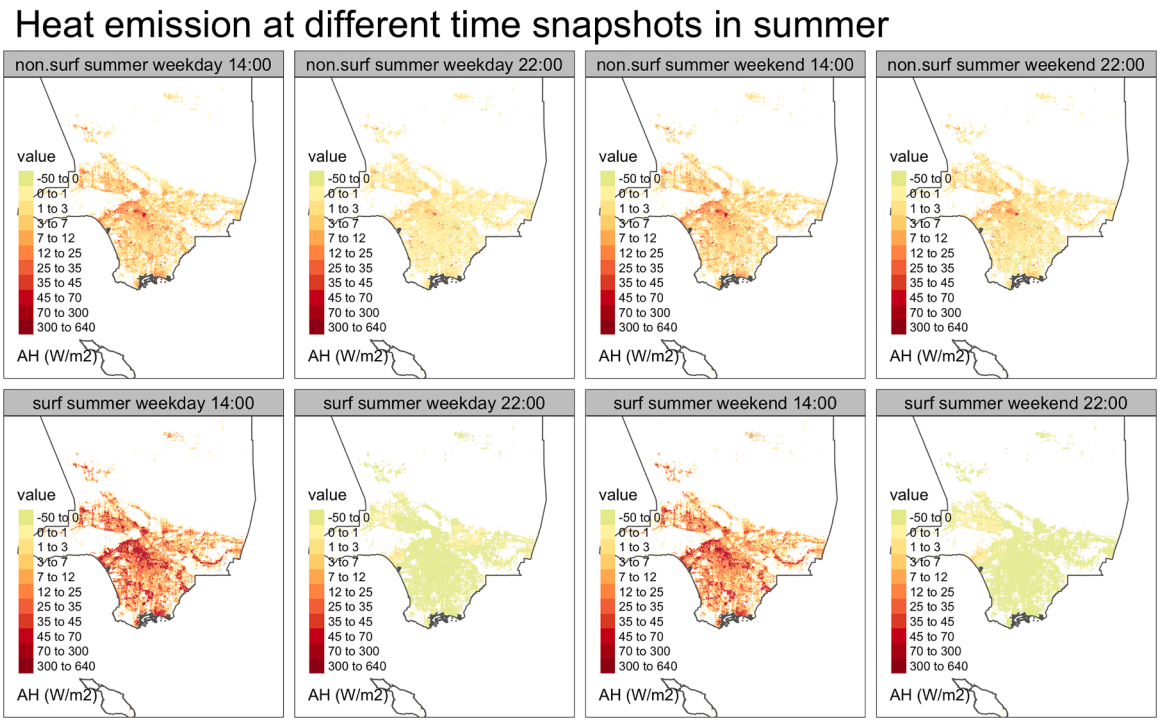

Fig. 15. Building anthropogenic heat snapshots in summer at noon and night on a weekday and a weekend day.

Table 6
Regression coefficients of anthropogenic heat on weather and building characteristics. Significant codes: $p < 0.001$ '***', $p < 0.01$ '**', $p < 0.05$ '*' The ones with "*" are statistically significant.

Building characteristics	Overall	Surface	HVAC	Zone
Ratio of industrial building	44.623***	43.942***	−4.812***	7.535***
Ratio of commercial building	10.043**	10.446**	2.979***	0.462
Ratio of residential building	−14.067***	−8.515*	−6.877***	−0.329
floor area ratio	208.806***	183.622***	41.840***	12.440***
Ratio of building with vintage around 2004	−11.653***	−11.472***	−1.256***	−0.163
Ratio of building with vintage around 2013	−14.735***	−11.967***	−4.800***	−1.501***

3.5. The impact of anthropogenic heat on the urban temperature rise

The impact of anthropogenic heat on urban temperature is analyzed for July 2018 by comparing the outdoor temperature simulated by WRF-UCM at 450 m resolution with and without representing anthropogenic heat. July month is selected as it is during summer when outdoor temperature increases are more concerning, and a heatwave was observed starting on July 6, 2018 (marked by the dash lines in Fig. 10Section 2.3.2) and lasted for about three days. As WRF-UCM explicitly models urban canopy including heat exchange between the building exterior surfaces and the urban environment, the AH impacts on urban temperature evaluated in this section only include the HVAC and zone AH components, excluding the surface AH component.

Fig. 19 shows the map view of average daily peak AH and AH-induced outdoor temperature changes. We can see the impact on daily min temperature is more severe and wider spread. The AH-induced change in average daily max temperature ranges from 0.2 to 0.6 °C. The highest increases are near downtown and Norwalk. AH-induced daily minimum temperature increase in July can be as high as 2.9 °C.

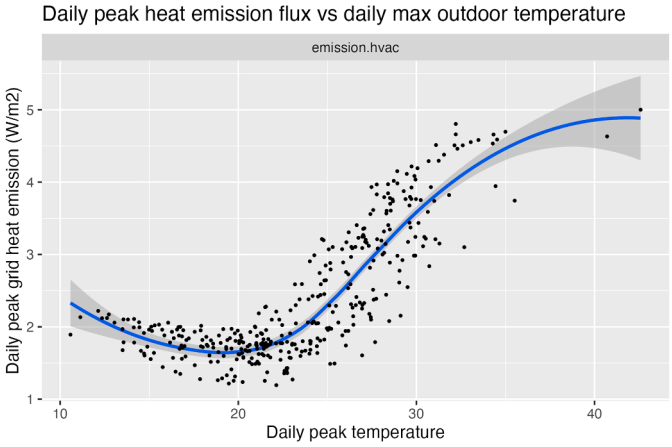

Fig. 16. Scatter plot of daily peak HVAC-induced AH and daily peak outdoor air temperature. Each point is a day, with peak AH and peak temperature averaged across all 450 m grid cells.

The highest increases are in neighborhoods around the Santa Monica Mountains.

A positive relationship is observed between building AH and temperature increase (Fig. 20). We split the temperature change-AH plot into high AH grids and low AH grids (with AH below the 95th percentile), as the AH distribution is very right skewed, making it hard to examine the relationship. Building AH causes a larger increase in daily minimum temperature than in daily maximum temperature. For the majority of the grid cells (below the 95th percentile), when the daily peak building AH increases by 100 W/m^2, the daily max ambient temperature increases by 0.02 °C, and the daily minimum temperature increases by about 0.16 °C. For high-AH grid cells, a 100 W/m^2 building AH increase corresponds to about 0.06 °C increase in daily maximum temperature and 0.14 °C increase in daily minimum temperature. The modest correlation between the spatial distributions of AH and changes

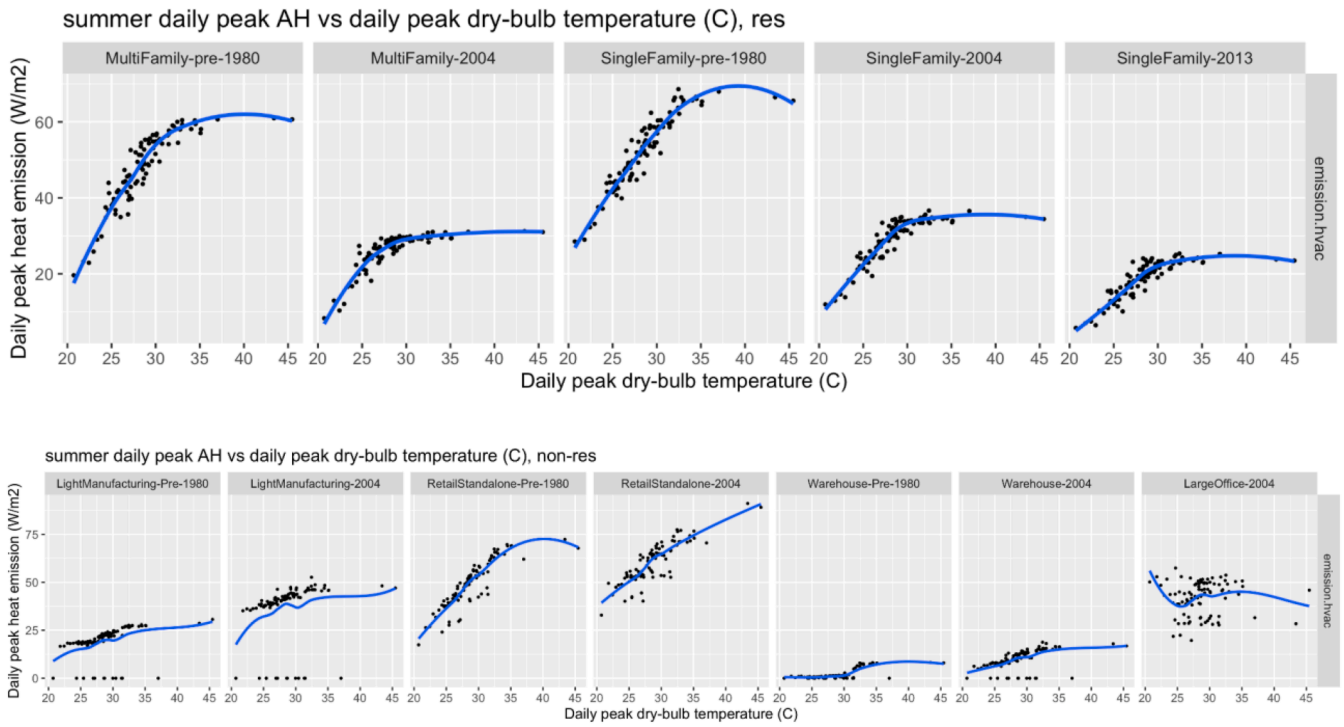

Fig. 17. Scatterplot of summer daily peak anthropogenic heat from HVAC and daily peak temperature for major residential buildings (top) and non-residential buildings (bottom) which constitute 90% of the building stock in LA County.

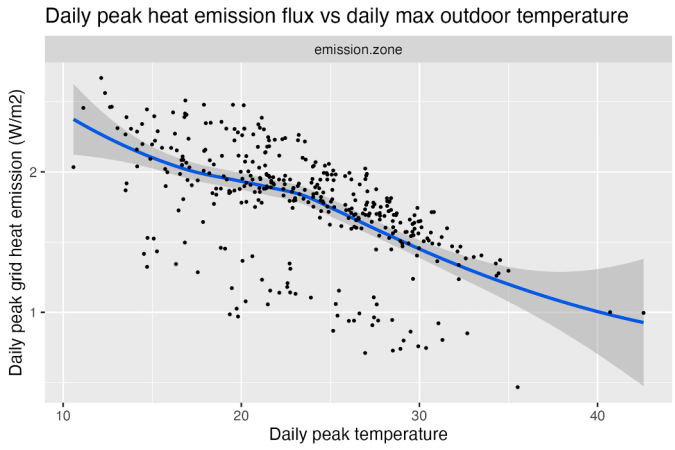

Fig. 18. Scatter plot of daily peak anthropogenic heat from zone air exchange, and daily peak temperature (bottom).

in air temperature could, in part, be attributed to the influence of wind. The movement of wind carries the heated air from regions with high AH to the adjacent downwind areas.

4. Discussion

4.1. Major findings

Building AH and energy consumption differ in multiple aspects. Annual total building AH is generally higher than its energy consumption. After excluding the surface component, the two become more similar but still quite different in their diurnal profile, especially in residential buildings, where the number of peaks and their timing differ substantially. Newer vintages affect energy and anthropogenic heat differently, whereas, in some non-residential buildings, such as full-service restaurants and small offices, newer buildings have smaller energy consumption but larger AH than older buildings.

Building AH has three components: surface, HVAC, and zone. The surface AH is the largest component, making up close to 80% of the total AH in residential buildings. Its ratio is lower in commercial and institutional buildings, accounting for 40% of the total AH, similar to the HVAC component.

Building anthropogenic heat exhibits substantial seasonal changes and diurnal variability as a result of the seasonality of its components. The surface and HVAC component is highest in summer, while the zone component is highest in Spring. Surface and building total AH peaks around noon and are at their lowest during the night, aligning well with the diurnal pattern of solar radiation. HVAC and zone AH peaks in the afternoon around 3pm, a little later than the temperature peaks around 1pm. These two components do not perfectly match that of outdoor temperature, as they are affected by both the outdoor conditions and building characteristics (e.g., thermal mass) and operation schedules. Anthropogenic heat emitted from zone air exchange is also affected by wind, which explains why it is highest in spring as spring has lower ambient temperature and higher wind speed.

Higher peak building anthropogenic heat is associated with higher building density (floor area ratio), higher ratio of industrial or commercial buildings, and more pre-1980 buildings. These explain the spatial patterns of the AH across LA County.

Non-surface building AH causes ambient temperature to increase in July 2018, a summer month with a heatwave starting on the 6th. The average change in daily maximum (daytime) temperature and minimum (nighttime) temperature is as high as 0.6 °C and 2.9 °C, respectively. Our analysis also highlights that wind patterns could play an important role in distributing the heated air from regions with high AH to the adjacent downwind areas.

4.2. Implications

The current study shows a large spatial variation in anthropogenic heat from buildings, where a small number of grid cells generate much

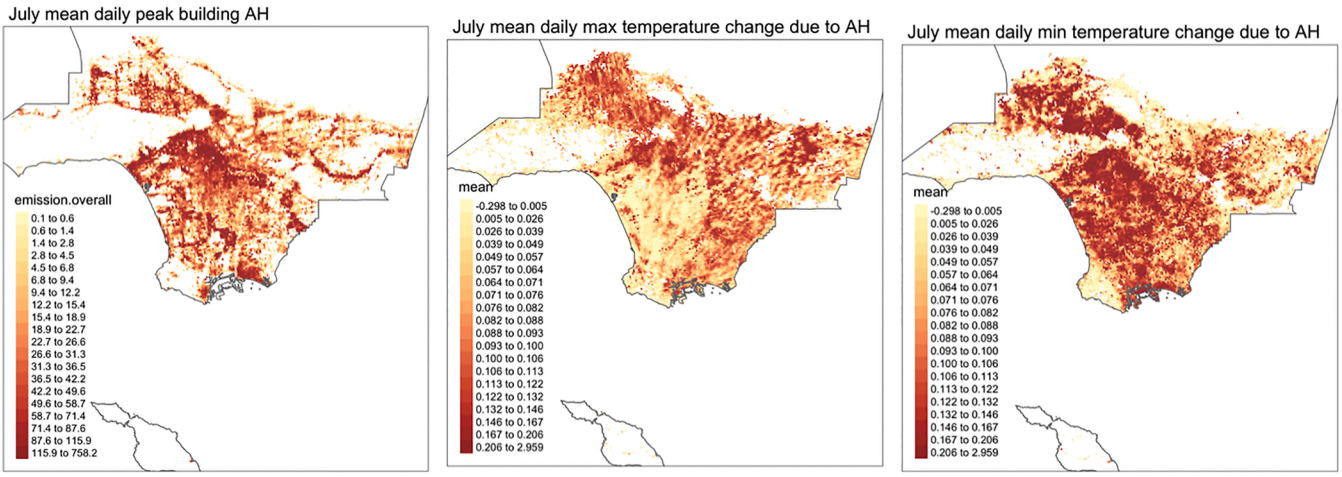

Fig. 19. Average daily max building AH (left), the average rise in daily maximum outdoor temperature due to AH (middle), the average rise in daily minimum outdoor temperature due to AH (right), restricted to grid cells with urban land use (land use id in category 23, 24, 25, 26) in central and southern LA County, excluding cloudy hours.

larger anthropogenic heat than the majority of grid cells. This suggests the importance of locating the hot spots and prioritizing interventions on them. For the LA County area, policymakers should target dense urban regions with a high percentage of industrial or commercial land uses. Reducing building AH can be achieved by upgrading energy efficiency of buildings to comply with California's newer building codes which will lead to less energy use and associated HVAC AH. However, trimming AH in industrial buildings could be challenging as their energy demand and resulting AH are heavily driven by the industrial process rather than their heating/cooling needs. As a result, it might be worth consideration to focus AH-reduction interventions on dense commercial or mixed-use neighborhoods around downtown and arrange industrial land uses in remote areas so that their AH-induced temperature increase would not affect the cooling demand of surrounding buildings. The impact of building energy efficiency upgrades on AH and energy are not always aligned, especially for non-residential buildings. The current study shows the effect of newer building vintages with higher energy efficiency levels generally reduces building energy consumption but not always on building anthropogenic heat. As a result, policy intervention decisions should not be solely based on its effect on energy and GHG reduction which is currently the driven goal of clean energy transition in cities. Their impact on AH should also be thoroughly evaluated to ensure measures and strategies for building decarbonization also reduce building AH and urban overheating during summer especially heatwaves in cities in warm and hot climates.

In the current LA building stock, residential and industrial buildings should focus more on reducing the surface AH, with strategies such as cool roofs and cool wall coatings. For commercial and institutional buildings, the focus should be on trimming HVAC-resulted AH during summer, with interventions that reduce cooling demand such as weatherization, shading, and envelope insulation, or cooling system efficiency improvement. The increase in ambient temperature causes increases in anthropogenic heat from HVAC operation and decreases in anthropogenic heat from surface convection and zone air exchange. This implies with global warming in the future, the anthropogenic heat from the HVAC component might account for a larger portion of the total building anthropogenic heat. It might become increasingly important to perform interventions reducing HVAC-resulted anthropogenic heat in residential and industrial buildings as well.

4.3. Limitations

There are limitations and uncertainties associated with the data and models used to generate the AH dataset. First, the LA County building stock data has some missing data; some buildings do not have the use type or have an invalid footprint polygon. Some buildings do not fall within the spatial domain covered by the WRF model. A small number of buildings are of a special use type that consumes energy mostly for industry processes such as food preparation or outdoor use. These three groups of buildings were not included in the modeling. Second, the prototype building energy models in EnergyPlus made assumptions about the building envelope, construction, and energy systems and their energy efficiency levels based on the requirements defined in the California Building Energy Efficiency Standards Title 24 and the U.S. nationwide ASHRAE Standard 90.1 for the building's construction year, which may not reflect individual building's actual energy efficiency or operation conditions. Third, the publicly available countywide building energy use data, used to quality check the simulated building energy use, are limited in their floor area ratio and the aggregation approach due to privacy concerns or the data collection process.

4.4. Future work

The building anthropogenic heat dataset is generated with a bottom-up simulation approach. To expand the analysis to other years or cities, a full set of simulations has to be redone. If the weather data is of finer spatial resolution (e.g., at 450 m), then the number of simulation runs could grow exponentially. Future studies could explore machine learning approaches (e.g., surrogate models) to speed up the simulation process while preserving the accuracy and flexibility of the simulation approach.

The current study analyzed the anthropogenic heat of the LA building stock under the current climate and building conditions. To provide better support for policy making, it would be important to analyze the impact of building decarbonization (electrification and energy efficiency upgrades) on anthropogenic heat. For long-term planning, it should also consider the impact of future climate. When grid cells producing 100 W/m^2 AH experience a 0 °C temperature increase and grid cells producing 10 W/m^2 experience a 3 °C temperature increase, there could be an equity issue. Future analysis could investigate the source of ambient temperature increase variability.

Future research is also needed for more detailed observations of AH and the processes that contribute to it, to help further develop and validate the models.

5. Conclusions

The current study investigates the building's anthropogenic heat

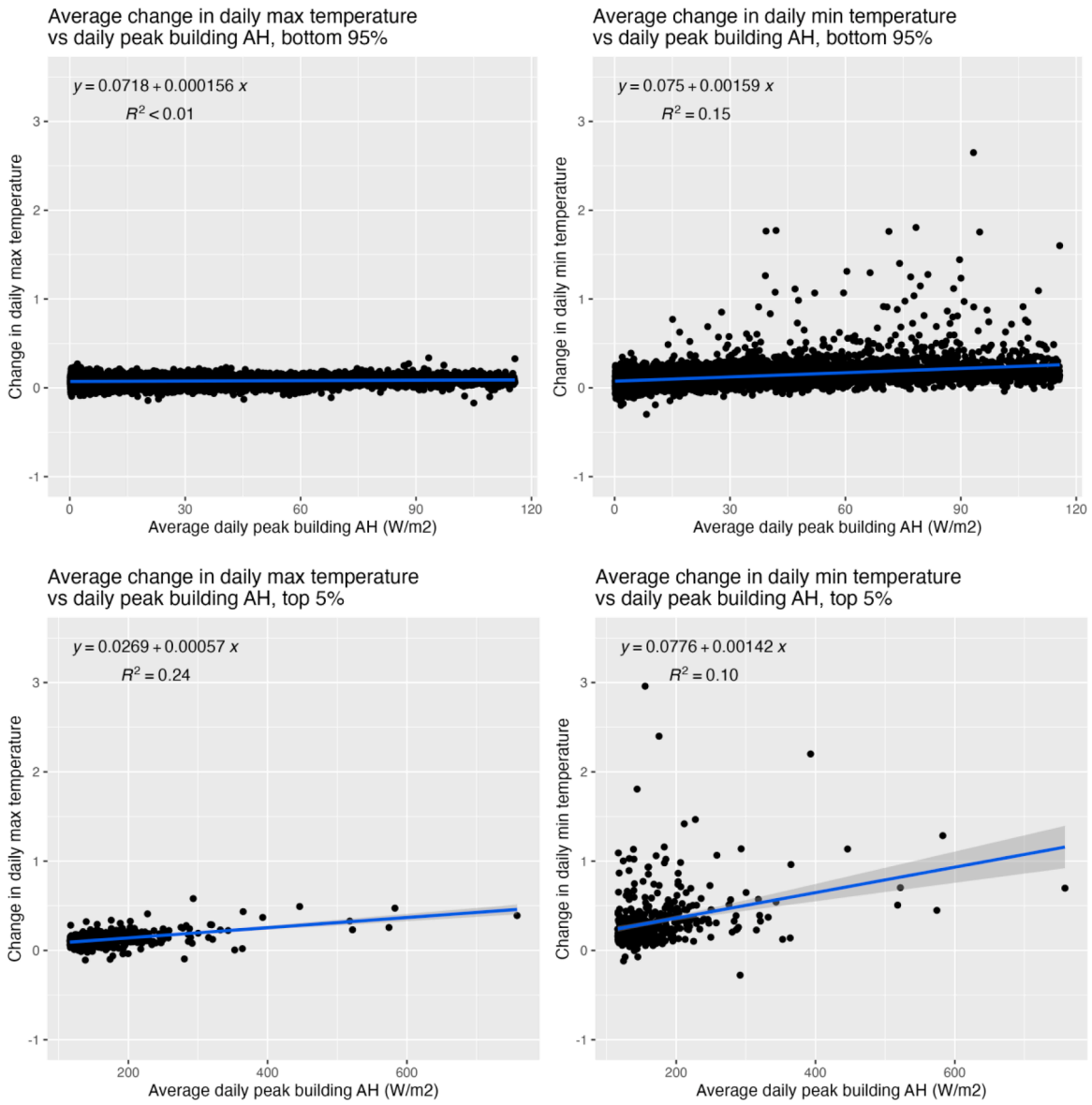

Fig. 20. July average daily peak AH vs the change in daily outdoor temperature range: AH vs change in daily maximum temperature (left), AH vs change in daily minimum temperature (right), for grid cells with building AH below the 95th percentile (top) and above the 95th percentile (bottom) across all grid cells. The plots are restricted to urban grid cells in central and south LA County. The temperature change statistics are restricted to non-cloudy hours.

components, timing, and their correlation with weather and building stock characteristics, and how building anthropogenic heat and outdoor temperature affect each other.

Buildings produce anthropogenic heat in three major components: through surface convection, through HVAC operation with heat rejection and air relief, and zone air exchange with the outdoor environment. These AH components have different magnitude and heat emission mechanisms and are affected by different environmental factors. The surface component is the largest and is mostly driven by solar radiation. HVAC and Zone anthropogenic heat is affected by both weather and building characteristics such as envelope, system efficiency, and operation schedules. As a result of this difference in AH producing mechanism, sometimes surface convection AH is not counted as part of the building anthropogenic heat.

Cooling and heating demand is the main driver of AH through HVAC operations. Daily peak HVAC-induced AH is lowest when the daily peak outdoor air temperature is around 20 °C; it increases when outdoors is colder or hotter. AH through zone air exchange decreases with outdoor temperature throughout the year.

Building anthropogenic heat leads to changes in outdoor air temperature. The change has large spatial and temporal variations. Grid cells with higher anthropogenic heat have a higher ambient temperature increase. For grid cells producing the same anthropogenic heat, the experienced temperature difference can differ by as much as 2 to 3 °C in daily minimum temperature, and up to 0.5 °C in daily maximum temperature. The building's anthropogenic heat during the heatwave in July 2018 can increase the maximum daytime outdoor air temperature by up to 0.6 °C, and increase the minimum nighttime outdoor air temperature by up to 2.9 °C. The significant increase in nighttime outdoor air temperature during the heatwave can lead to overheating risks and poor sleeping quality of residents without air-conditioning, which becomes a climate equity issue, especially for underserved communities with limited or no air-conditioning.

6. Data access

The hourly anthropogenic heat dataset produced in the current study has been uploaded to the MSD-Live website for public access; users can

download data through this link: https://doi.org/10.57931/1892041, or https://data.msdlive.org/records/zxs8c-kpv35.

The GitHub repository https://github.com/IMMM-SFA/xu_etal_2022_sdata holds the data record documentation and data processing steps and scripts.

The WRF-UCM data used in the current study is publicly accessible via Globus with a copy stored and minted in the MSD-Live data repository (https://doi.org/10.57931/1885756) which could be used to reproduce our results. Instructions for downloading the data, as well as additional information regarding the dataset and available variables can be found at a data landing page (https://tgw-data.msdlive.org).

CRediT authorship contribution statement

Yujie Xu: Writing – review & editing, Writing – original draft, Visualization, Validation, Software, Methodology, Investigation, Formal analysis, Data curation. **Pouya Vahmani:** Writing – review & editing, Writing – original draft, Visualization, Validation, Software, Methodology, Investigation, Formal analysis, Data curation, Conceptualization. **Andrew Jones:** Writing – review & editing, Writing – original draft, Supervision, Resources, Project administration, Methodology, Funding acquisition, Conceptualization. **Tianzhen Hong:** Writing – review & editing, Writing – original draft, Supervision, Methodology, Conceptualization.

Declaration of competing interest

The authors declare that they have no known competing financial interests or personal relationships that could have appeared to influence the work reported in this paper.

Data availability

The dataset is open and published.

Acknowledgments

This research was supported by the U.S. Department of Energy, Office of Science, as part of research in the MultiSector Dynamics, Earth and Environmental System Modeling Program. This research used resources of the National Energy Research Scientific Computing Center (NERSC), a User Facility supported by the Office of Science of the U.S. Department of Energy under Contract No. DE-AC02–05CH11231. The authors appreciate the technical support of Kaiyu Sun for generating the prototype building models from CBES and OpenStudio Standards Gem. The authors thank Stephanie Pincetl of the University of California, Los Angeles for providing the annual building energy use data aggregated at the census tract level. The authors appreciate Cam-Giang Nguyen and Julianne Alontave of the California Energy Commission for providing the sector breakdown data for county-wide energy use.

References

Alhazmi, M., Sailor, D. J., & Anand, J. (2022). A new perspective for understanding actual anthropogenic heat emissions from buildings. *Energy and Buildings, 258*, Article 111860. https://doi.org/10.1016/j.enbuild.2022.111860

Andreatta, R., & Kirksey, T. (2018). *Southern California Heat Wave July 2018*. July 6. Climate Signals https://www.climatesignals.org/events/southern-california-heat-wave-july-2018.

Block, A., Keuler, K., & Schaller, E. (2004). Impacts of anthropogenic heat on regional climate patterns. *Geophysical Research Letters, 31*(12). https://doi.org/10.1029/2004GL019852

California Energy Commission. (2020). *Electricity consumption by county*. California Energy Commission. https://ecdms.energy.ca.gov/elecbycounty.aspx.

Chen, F., Kusaka, H., Bornstein, R., Ching, J., Grimmond, C., Grossman-Clarke, S., et al. (2011). The integrated WRF/urban modelling system: Development, evaluation, and applications to urban environmental problems. *International Journal of Climatology, 31*(2), 273–288.

Chen, W., Zhou, Y., Xie, Y., Chen, G., Ding, K. J., & Li, D. (2022). Estimating spatial and temporal patterns of urban building anthropogenic heat using a bottom-up city building heat emission model. *Resources, Conservation and Recycling, 177*, Article 105996. https://doi.org/10.1016/j.resconrec.2021.105996

Ching, J., Brown, M., Burian, S., Chen, F., Cionco, R., Hanna, A., et al. (2009). National Urban Database and Access Portal Tool. *Bulletin of the American Meteorological Society, 90*(8), 1157–1168. https://doi.org/10.1175/2009BAMS2675.1

Dhakal, S., Hanaki, K., & Hiramatsu, A. (2004). Heat discharges from an office building in Tokyo using DOE-2. *Energy Conversion and Management, 45*(7), 1107–1118. https://doi.org/10.1016/j.enconman.2003.08.012

Dong, Y., Varquez, A. C. G., & Kanda, M. (2017). Global anthropogenic heat flux database with high spatial resolution. *Atmospheric Environment, 150*, 276–294. https://doi.org/10.1016/j.atmosenv.2016.11.040

Hersbach, H., Bell, B., Berrisford, P., Hirahara, S., Horányi, A., Muñoz-Sabater, J., et al. (2020). The ERA5 global reanalysis. *Quarterly Journal of the Royal Meteorological Society, 146*(730), 1999–2049.

Homer, C. H., Fry, J. A., & Barnes, C. A. (2012). The national land cover database. *US Geological Survey Fact Sheet, 3020*(4), 1–4.

Hong, T., Ferrando, M., Luo, X., & Causone, F. (2020). Modeling and analysis of heat emissions from buildings to ambient air. *Applied Energy, 277*, Article 115566. https://doi.org/10.1016/j.apenergy.2020.115566

Hong, T., Piette, M. A., Chen, Y., Lee, S. H., Taylor-Lange, S. C., Zhang, R., et al. (2015). Commercial Building Energy Saver: An energy retrofit analysis toolkit. *Applied Energy, 159*, 298–309. https://doi.org/10.1016/j.apenergy.2015.09.002

Janjić, Z. I.. (1994). The Step-Mountain Eta Coordinate Model: Further Developments of the Convection, Viscous Sublayer, and Turbulence Closure Schemes. *Monthly Weather Review, 122*(5), 927–945. https://doi.org/10.1175/1520-0493(1994)122<0927:TSMECM>2.0.CO;2

Kikegawa, Y., Genchi, Y., Yoshikado, H., & Kondo, H. (2003). Development of a numerical simulation toward comprehensive assessments of urban warming countermeasures including their impacts upon the urban buildings energy demands (in Japanese). *Applied Energy, 76*, 449–466. https://doi.org/10.1016/S0306-2619(03)00009-6

Kusaka, H., Kondo, H., Kikegawa, Y., & Kimura, F. (2001). A simple single-layer urban canopy model for atmospheric models: Comparison with multi-layer and slab models. *Boundary-Layer Meteorology, 101*(3), 329–358.

Luo, X., Vahmani, P., Hong, T., & Jones, A. (2020). City-Scale Building Anthropogenic Heating during Heat Waves. *Atmosphere, 11*(11), Article 11. https://doi.org/10.3390/atmos11111206. Article.

Mesinger, F. (2010). Several PBL parameterization lessons arrived at running an NWP model. *IOP Conference Series: Earth and Environmental Science, 13*(1), Article 012005. https://doi.org/10.1088/1755-1315/13/1/012005

Monin, A. S., & Obukhov, A. M. (1954). Basic laws of turbulent mixing in the surface layer of the atmosphere. *Contrib. Geophys. Inst. Acad. Sci. USSR, 151*(163), e187.

Nie, W. S., Sun, T., & Ni, G. H. (2014). Spatiotemporal characteristics of anthropogenic heat in an urban environment: A case study of Tsinghua Campus. *Building and Environment, 82*, 675–686. https://doi.org/10.1016/j.buildenv.2014.10.011

NREL. (2022). *OpenStudio-Standards [Ruby]*. National Renewable Energy Laboratory. https://github.com/NREL/openstudio-standards (Original work published 2014).

Perkins-Kirkpatrick, S. E., & Lewis, S. C. (2020). Increasing trends in regional heatwaves. *Nature Communications, 11*(1), Article 1. https://doi.org/10.1038/s41467-020-16970-7

Quah, A. K. L., & Roth, M. (2012). Diurnal and weekly variation of anthropogenic heat emissions in a tropical city, Singapore. *Atmospheric Environment, 46*, 92–103. https://doi.org/10.1016/j.atmosenv.2011.10.015

Sailor, D. J.. (2011). A review of methods for estimating anthropogenic heat and moisture emissions in the urban environment. *International Journal of Climatology, 31*(2), 189–199. https://doi.org/10.1002/joc.2106

Sailor, D. J., & Lu, L. (2004). A top–down methodology for developing diurnal and seasonal anthropogenic heating profiles for urban areas. *Atmospheric Environment, 38*(17), 2737–2748. https://doi.org/10.1016/j.atmosenv.2004.01.034

Skamarock, W. C., Klemp, J. B., Dudhia, J., Gill, D. O., Liu, Z., Berner, J., et al. (2019). A description of the advanced research WRF model version 4. *National Center for Atmospheric Research: Boulder, CO, USA, 145*, 145.

Smith, C., Lindley, S., & Levermore, G. (2009). Estimating spatial and temporal patterns of urban anthropogenic heat fluxes for UK cities: The case of Manchester. *Theoretical and Applied Climatology, 98*(1), 19–35. https://doi.org/10.1007/s00704-008-0086-5

Sun, K., Specian, M., & Hong, T. (2020). Nexus of thermal resilience and energy efficiency in buildings: A case study of a nursing home. *Building and Environment, 177*, Article 106842. https://doi.org/10.1016/j.buildenv.2020.106842

Thompson, G., Field, P. R., Rasmussen, R. M., & Hall, W. D. (2008). Explicit Forecasts of Winter Precipitation Using an Improved Bulk Microphysics Scheme. Part II: Implementation of a New Snow Parameterization. *Monthly Weather Review, 136*(12), 5095–5115. https://doi.org/10.1175/2008MWR2387.1

U.S. Census Bureau. (2022). *QuickFacts*. July. U.S. Census Bureau https://www.census.gov/quickfacts/fact/table/losangelescountycalifornia,CA/PST045222.

U.S. Department of Energy. (2022). EnergyPlus [Computer software]. https://energyplus.net/.

U.S. Energy Information Administration. (2021). *Manufacturing energy consumption survey*. December. U.S. Energy Information Administration - EIA - Independent Statistics and Analysis https://www.eia.gov/consumption/manufacturing/.

UCLA California Center for Sustainable Communities. (2020). Energy Atlas. https://energyatlas.ucla.edu/about.

Vahmani, P., Jones, A. D., & Patricola, C. M. (2019). Interacting implications of climate change, population dynamics, and urban heat mitigation for future exposure to heat

extremes. *Environmental Research Letters, 14*(8), Article 084051. https://doi.org/10.1088/1748-9326/ab28b0

Vahmani, P., Luo, X., Jones, A., & Hong, T. (2022). Anthropogenic heating of the urban environment: An investigation of feedback dynamics between urban micro-climate and decomposed anthropogenic heating from buildings. *Building and Environment, 213*, Article 108841. https://doi.org/10.1016/j.buildenv.2022.108841

Wang, K., Aktas, Y. D., Malki-Epshtein, L., Wu, D., & Ammar Bin Abdullah, M. F. (2022). Mapping the city scale anthropogenic heat emissions from buildings in Kuala Lumpur through a top-down and a bottom-up approach. *Sustainable Cities and Society, 76*, Article 103443. https://doi.org/10.1016/j.scs.2021.103443

Wickham, J. D., Stehman, S. V., Gass, L., Dewitz, J., Fry, J. A., & Wade, T. G. (2013). Accuracy assessment of NLCD 2006 land cover and impervious surface. *Remote Sensing of Environment, 130*, 294–304. https://doi.org/10.1016/j.rse.2012.12.001

Xu, C., Ao, X., Zhao, B., & Pei, G. (2021). A novel selective emissivity spectrum for radiative sky cooling. *Solar Energy Materials and Solar Cells, 232*, Article 111380. https://doi.org/10.1016/j.solmat.2021.111380

Yang, J., Wang, Z. H., Chen, F., Miao, S., Tewari, M., Voogt, J. A., et al. (2015). Enhancing hydrologic modelling in the coupled weather research and forecasting–urban modelling system. *Boundary-Layer Meteorology, 155*(1), 87–109.

Zheng, Y., & Weng, Q. (2018). High spatial- and temporal-resolution anthropogenic heat discharge estimation in Los Angeles County, California. *Journal of Environmental Management, 206*, 1274–1286. https://doi.org/10.1016/j.jenvman.2017.07.047

Zhou, Y., Weng, Q., Gurney, K. R., Shuai, Y., & Hu, X. (2012). Estimation of the relationship between remotely sensed anthropogenic heat discharge and building energy use. *ISPRS Journal of Photogrammetry and Remote Sensing, 67*, 65–72. https://doi.org/10.1016/j.isprsjprs.2011.10.007